Title

Cross-species functional diversity within the PIN auxin efflux protein family

Authors

Devin Lee O'Connor[1,^], Samuel Elton[1*], Fabrizio Ticchiarelli[1*], Mon Mandy Hsia[2], John Vogel[3,4], Ottoline Leyser[1].

Affiliations

[1]Sainsbury Laboratory University of Cambridge, Cambridge, UK.

[2]USDA-ARS Western Regional Research Center, Albany, CA.

[3]U.S. Department of Energy Joint Genome Institute, Walnut Creek, CA.

[4]Department of Plant and Microbial Biology, University of California, Berkeley, CA.

*These authors contributed equally.

^Author for Correspondence: Devin Lee O'Connor devin.oconnor@slcu.cam.ac.uk

Abstract

In Arabidopsis, development during flowering is coordinated by transport of the hormone auxin mediated by polar-localized PIN-FORMED1 (AtPIN1). However Arabidopsis has lost a PIN clade sister to AtPIN1, Sister-of-PIN1 (SoPIN1), which is conserved in flowering plants. We previously proposed that the AtPIN1 organ initiation and vein patterning functions are split between the SoPIN1 and PIN1 clades in grasses. Here we show that in the grass Brachypodium *sopin1* mutants have organ initiation defects similar to Arabidopsis *atpin1*, while loss of *PIN1* function in Brachypodium has little effect on organ initiation but alters stem growth. Heterologous expression of Brachypodium SoPIN1 and PIN1b in Arabidopsis provides further evidence of functional specificity. SoPIN1 but not PIN1b can mediate flower formation in null *atpin1* mutants, although both can complement a missense allele. The behavior of SoPIN1 and PIN1b in Arabidopsis illustrates how membrane and tissue-level accumulation, transport activity, and interaction contribute to PIN functional specificity.

Introduction

The plant hormone auxin is an essential mobile signal controlling growth and patterning throughout plant development (Leyser, 2010). Auxin can passively enter cells triggering a vast array of downstream signaling events (Wang and Estelle, 2014), but it cannot easily exit the cell without active transport (Raven, 1975; Rubery and Sheldrake, 1974). As a result, directional efflux mediated by the polar-localized PIN-FORMED (PIN) efflux carriers can organize auxin flows and accumulation patterns, creating concentration maxima and paths of transport that regulate growth, position organs and pattern tissues

39 (Adamowski and Friml, 2015). Because auxin itself feeds back to regulate PIN-mediated
40 transport both transcriptionally and post-transcriptionally (Leyser, 2006), the transport
41 system shows remarkable robustness and plasticity. For example compensatory
42 changes in PIN abundance between PIN family members can mitigate PIN loss-of-
43 function mutant phenotypes (Blilou et al., 2005; Paponov et al., 2005; Vieten et al.,
44 2005), environmental inputs can trigger tissue-level changes in PIN abundance and
45 polarity leading to altered plant growth (Habets and Offringa, 2014), and auxin transport
46 paths can be reorganized in response to injury (Sauer et al., 2006; Xu et al., 2006) or
47 spontaneously in tissue culture (Gordon et al., 2007). The self-organizing properties of
48 the auxin transport system gives this patterning mechanism extraordinary versatility and
49 allows it to coordinate both local and long-range communication in plants.

50 The correct initiation and positioning of organs (leaves, flowers, stems) in the growing
51 tip, or shoot apical meristem, of *Arabidopsis thaliana* (Arabidopsis) plants requires the
52 action of the PIN-FORMED1 (AtPIN1) auxin efflux carrier (Okada et al., 1991). AtPIN1
53 is targeted to the plasma membrane and polarized in cells (Gälweiler et al., 1998). In
54 the meristem epidermis polarization of AtPIN1 in neighboring cells converges around
55 the initiation sites of new organs, suggesting that polarized AtPIN1 concentrates auxin
56 into local maxima causing organ initiation (Benková et al., 2003; Heisler et al., 2005;
57 Reinhardt et al., 2003). Accordingly in *atpin1* loss-of-function mutants or if auxin
58 transport is pharmacologically inhibited, organ initiation is aborted but it can be rescued
59 with local auxin application to the meristem flank (Reinhardt et al., 2003; Reinhardt et al.,
60 2000). Organ initiation in *atpin1* mutants can also be rescued with epidermal-specific
61 AtPIN1 expression (Bilsborough et al., 2011) and reducing AtPIN1 function specifically

62 in the epidermis compromises organ positioning and initiation (Kierzkowski et al., 2013),
63 demonstrating the importance of convergent AtPIN1 polarization in the epidermis during
64 organ formation.

65 The recurrent formation of AtPIN1 convergence points surrounding auxin maxima in the
66 meristem epidermis has been the focus of several computational models that attempt to
67 explain how auxin feeds back on its own transport via AtPIN1 to concentrate auxin and
68 control organ spacing (Abley et al., 2016; Bayer et al., 2009; Bhatia et al., 2016; Heisler
69 et al., 2010; Jönsson et al., 2006; Smith et al., 2006; Stoma et al., 2008). However
70 AtPIN1 is also expressed during the patterning of the vascular strands formed
71 coincident with organ positioning, and in these sub-epidermal cells AtPIN1 is polarized
72 rootward away from the presumed auxin maxima, suggesting that AtPIN1 polarity with
73 respect to auxin concentration may vary across tissues or over developmental time
74 (Bayer et al., 2009).

75 Indeed AtPIN1 has several functions post organ initiation that are not necessarily
76 associated with convergent polarization patterns (Gälweiler et al., 1998; Scarpella et al.,
77 2006). AtPIN1 is not required for organ formation during the vegetative phase. Mutants
78 lacking AtPIN1 form leaves but they are misplaced and have severe morphological and
79 vascular defects similar to those observed upon pharmacological inhibition of auxin
80 transport, suggesting an important role for AtPIN1 in post-initiation morphogenesis and
81 vein patterning in leaves (Guenot et al., 2012; Sawchuk et al., 2013; Verna et al., 2015).
82 Furthermore in mature tissues AtPIN1 is polarized rootward in vascular-associated cells
83 and is required for efficient long distance transport of auxin down the shoot in the polar
84 auxin transport stream and this has been proposed to play an important role in the

85 regulation of shoot branching (Bennett et al., 2016; Bennett et al., 2006; Gälweiler et al.,
86 1998; Shinohara et al., 2013). Mutations in other PIN family members in combination
87 with *atpin1* mutants suggest further functions in embryo development, root development
88 and during plant growth responses to light and gravity (Leyser, 2005). Unfortunately the
89 myriad roles for AtPIN1 during inflorescence development are genetically obscured by
90 the severity of *atpin1* organ initiation defects.

91 We previously showed that all sampled flowering plants outside of the Brassicacea
92 family have a clade of PIN proteins phylogenetically sister to the PIN1 clade (The Sister-
93 of-PIN1 or SoPIN1 clade), while Arabidopsis and other Brassicacea species have lost
94 this clade (O'Connor et al., 2014). During initiation of the lemma, a leaf-like floral organ
95 in the grass *Brachypodium distachyon* (Brachypodium), which has both PIN1 and
96 SoPIN1 clades, SoPIN1 is highly expressed in the epidermis, polarizes towards
97 presumed auxin maxima, and forms convergent polarization patterns, suggesting a role
98 in creating the auxin maxima required for organ initiation in the shoot. In contrast, the
99 duplicate Brachypodium PIN1 clade members, PIN1a and PIN1b, are not highly
100 expressed in the epidermis, orient away from presumed auxin maxima and are primarily
101 expressed during patterning in the sub-epidermal tissues. Thus the combined
102 expression domains and polarization behaviors of SoPIN1, PIN1a, and PIN1b in
103 Brachypodium largely recapitulate those observed for AtPIN1 alone in Arabidopsis.

104 The dynamic localization and polarization patterns of the Brachypodium SoPIN1 and
105 PIN1 clades can be modeled with two different polarization modes with respect to auxin.
106 PIN behaviors can be captured by a model in which SoPIN1 polarizes “up-the-gradient”
107 towards the neighboring cell with the highest auxin concentration, while PIN1a and

108 PIN1b polarize “with-the-flux” accumulating in the membrane with the highest net auxin
109 efflux (O'Connor et al., 2014). Both polarization modes were previously applied to
110 AtPIN1 in order to capture the switch in polarity observed during organ initiation and
111 vein patterning, first orienting toward the auxin maximum during convergence point
112 formation, then orienting away from the maximum below the epidermis during vein
113 patterning (Bayer et al., 2009). These localization and modeling results suggest that in
114 most angiosperm species the organ placement and vascular patterning functions
115 attributed to AtPIN1 in Arabidopsis are split between the PIN1 and SoPIN1 clades and
116 that these two clades have different polarization properties with respect to auxin.

117 Exploring this hypothesis, here we present the functional analysis of both the SoPIN1
118 and PIN1 protein clades in Brachypodium, a species with the canonical two-clade family
119 structure. We show that SoPIN1 and the PIN1 clade members PIN1a and PIN1b have
120 different functions during Brachypodium development, with SoPIN1 being required for
121 organ initiation during the flowering phase, and PIN1a and PIN1b regulating stem
122 growth. Using heterologous expression in Arabidopsis we show that the SoPIN1 and
123 PIN1b proteins have different accumulation, polarization, and transport behaviors that
124 result in different functional properties independent of transcriptional context. In addition
125 to elucidating several ways in which PIN family members can be functionally distinct,
126 these results suggest that the Arabidopsis AtPIN1 protein represents an example of an
127 evolutionary phenomenon the opposite of subfunctionalisation in which protein functions
128 are amalgamated into a single protein rather than diversified amongst paralogs. AtPIN1
129 has a repertoire of roles and associated polarization behaviors that are distributed
130 among several clades of PIN proteins in most flowering plants.

131 # Results

132 ## The SoPIN1 and PIN1 clades have different functions in
133 Brachypodium

134 We targeted Brachypodium SoPIN1, PIN1a and PIN1b with gene-specific Clustered
135 Regularly Interspaced Short Palindromic Repeats (CRISPR) and for all three genes
136 recovered independent single base-pair lesions causing frame shifts and premature
137 stop codons (Figure 1A). The wild-type Brachypodium inflorescence meristem normally
138 makes several lateral spikelet meristems (lsm) before producing a terminal spikelet
139 meristem (tsm) (Figure 1B)(Derbyshire and Byrne, 2013). Both lateral and terminal
140 spikelet meristems are consumed in the production of florets (Figure 1D, 1F). The
141 *sopin1-1* inflorescence meristems had severe organ and spikelet branch initiation
142 defects (Figure 1C), which resulted in reduced total whole-plant spikelet number (Figure
143 1H). When spikelets did form, *sopin1-1* spikelet meristems were often devoid of new
144 organs (Figure 1E) and very few recognizable florets were produced (Figure 1I). In
145 support of the *sopin1-1* lesion being responsible for these varied inflorescence
146 phenotypes, we complemented inflorescence development and seed set by crossing
147 *sopin1-1* to the previously published SoPIN1-CITRINE fusion line (Figure 1 –
148 supplement 1)(O'Connor et al., 2014). The pleotropic defects displayed by *sopin1-1* in
149 the inflorescence are remarkably similar to loss-of-function *pin1* mutants in *Arabidopsis*
150 (Okada et al., 1991) and *Cardamine hirsuta* (Barkoulas et al., 2008).

151 In wild-type spikelet meristems SoPIN1 convergence point formation is coincident with
152 an increase in the auxin signaling reporter DR5 (O'Connor et al., 2014), as well as a

153 decrease in the nuclear auxin response reporter protein DII-Venus (Brunoud et al.,
154 2012) (DII) (Figure 1J), which functions in Brachypodium and is degraded in the
155 presence of auxin in spikelet meristems (Figure 1 - supplement 2). In *sopin1-1*
156 meristems DII accumulation was uniformly high for long stretches of the epidermis and
157 the patterned reduction of DII both in the meristem epidermis and internally failed to
158 occur, suggesting a failure to organize auxin maxima (Figure 1K arrow).

159 In contrast to the severe defects of *sopin1-1*, organ initiation in *pin1a-1* and *pin1b-1*
160 single mutants was largely unaffected. The mature inflorescences of both *pin1a-1* and
161 *pin1b-1* had normal spikelets (Figure 1F) and spikelet meristem morphology was
162 indistinguishable from wild-type (Figure 1G). Mutant *pin1a-1* plants appeared visually
163 wild-type but we measured a slight increase in total spikelet number (Figure 1H). Mutant
164 *pin1b-1* plants were similar to wild-type with respect to both spikelet and floret numbers
165 (Figure 1H, 1I) but often had bent apical internodes (Figure 1F arrowhead). While *pin1a-*
166 *1* and *pin1b-1* single mutants had no clear organ initiation defects they showed changes
167 in internode length (Figure 2). Plant stature in *pin1a-1* mutants was largely
168 indistinguishable from wild-type (Figure 2B) but we measured a small reduction in the
169 length of the I4 internode (Figure 2E). In contrast *pin1b-1* plants were easily
170 distinguished from wild-type because of a significant increase in internode length at the
171 base of the plant, resulting in greater overall plant height (Figure 2E). The elongated
172 basal internodes and bent stems of *pin1b-1* resulted in a less compact plant architecture
173 compared to the other genotypes (Figure 2C). The increase in basal internode length in
174 *pin1b-1* single mutants was rescued by the previously published PIN1b-CITRINE
175 florescent reporter (O'Connor et al., 2014) (Figure 2 – supplement 1).

176 The PIN1a and PIN1b duplication is specific to, but conserved within the grasses
177 (O'Connor et al., 2014). Thus we suspected these two genes would show a degree of
178 genetic redundancy. Indeed *pin1a-1/pin1b-1* (*pin1a/b*) double mutants showed a
179 synergistic phenotype with severely reduced plant height (Figure 2D) resulting primarily
180 from reduced internode growth in the upper internodes (Figure 2E). However despite
181 loss of both PIN1a and PIN1b function, *pin1a/b* double mutants made normal spikelet
182 meristems (Figure 1G), had a wild-type total spikelet number (Figure 1H) and showed
183 only a small reduction in floret number in the terminal spikelet (Figure 1I). In addition
184 unlike *sopin1-1* plants, *pin1a/b* double mutants set ample seed.

185 Combined these phenotypes provide further support for functional distinction between
186 the SoPIN1 and PIN1 clades and indicate that while the PIN1 clade is expendable for
187 organ initiation in Brachypodium, it is involved in the regulation of internode growth.

188

189 AtPIN1, SoPIN1 and PIN1b accumulate differently in Arabidopsis 190 under the same transcriptional control

191 During organ formation in the Brachypodium shoot, expression of both SoPIN1 and
192 PIN1b precedes PIN1a, which only accumulates significantly at the sites of vein
193 formation after the organs begin to grow (O'Connor et al., 2014). In the earliest stages
194 of initiation prior to the periclinal cell divisions that are the hallmark of morphogenesis,
195 SoPIN1 forms convergent polarization patterns around the presumed auxin maxima in
196 the meristem epidermis, while PIN1b is expressed internally and orients away from the
197 maxima (O'Connor et al., 2014). Because of their early expression, opposing

198 polarization patterns and their clear single-mutant phenotypes in Brachypodium, we
199 focused on characterizing SoPIN1 and PIN1b as representatives of the SoPIN1 and
200 PIN1 clades.

201 The difference between the *sopin1-1* and *pin1b-1* phenotypes in Brachypodium could
202 be due to their different expression patterns and not necessarily to differences in their
203 polarization with respect to auxin concentration or flux as previously hypothesized
204 (O'Connor et al., 2014). In order to assess the functional differences between the
205 proteins independent of transcriptional context, we expressed both Brachypodium
206 proteins tagged with CITRINE (a YFP derivative) in wild-type Arabidopsis (Columbia,
207 Col-0) under the control of a 3.5kb Arabidopsis *PIN1* promoter fragment which includes
208 sequences known to drive PIN1 expression sufficient to complement *pin1* mutants
209 (*proAtPIN1*) (Benková et al., 2003; Heisler et al., 2005). In the Arabidopsis inflorescence
210 meristem, wild-type AtPIN1 forms convergent polarization patterns that mark the sites of
211 initiating flower primordia (Figure 3A). Remarkably, despite the loss of the SoPIN1 clade
212 from Arabidopsis, Brachypodium SoPIN1 also created clear convergent polarization
213 patterns in Arabidopsis inflorescence meristems but was less abundant in the central
214 domain of the apical dome (Figure 3B, 25 of 27 meristems from 4 independent
215 transgenic events). Similar to AtPIN1, SoPIN1 protein abundance was highest in the
216 meristem epidermis and SoPIN1 convergence points were most clearly observed
217 surrounding I2 and I1 primordia (Figure 3B). Below the epidermis wild-type AtPIN1
218 accumulates in small groups of cells that will become the vasculature (Figure 3 –
219 supplement 1 panel A arrows). In contrast sub-epidermal SoPIN1 accumulated in an ill-
220 defined ring shape surrounding the meristem central domain without distinct foci of

221 expression (Figure 3 – supplement 1 panel B, 15 of 23 meristems from 4 independent
222 transgenic events).

223 In contrast to both AtPIN1 and SoPIN1, under the same promoter significant PIN1b
224 accumulation was absent from the meristem epidermis in 19 of 29 meristems from 7
225 independent transgenic events. In the meristems where PIN1b accumulated in the
226 epidermis it did not show clear convergent polarization patterns and its polarity was
227 often unclear (Figure 3C, 10 meristems from 2 events). Within initiating organs PIN1b
228 often localized to punctate vesicular bodies inside cells, not in the cell membrane
229 (Figure 3C arrowhead). PIN1b accumulation remained low just below the meristem
230 apex, but in contrast to SoPIN1, PIN1b formed defined domains around the presumptive
231 developing vascular bundles similar to AtPIN1 (Figure 3 – supplement 1 panel C
232 arrows). The lack of PIN1b protein in the meristem epidermis was not due to silencing of
233 the transgene in these lines because we observed abundant PIN1b protein in the
234 developing vasculature below the apex, even in plants where the meristem had no
235 detectable epidermal expression (Figure 3F) (8 samples from 4 events). In contrast,
236 AtPIN1 and SoPIN1 accumulated in both the vasculature and the epidermis in these
237 more mature tissues (Figure 3D, 3E) although SoPIN1 seemed more abundant in the
238 epidermis than AtPIN1 (see arrows) (SoPIN1 - 5 samples from 2 events).

239 In order to determine whether there were similar tissue-level differences in protein
240 accumulation in mature tissues where AtPIN1 is implicated in branch control, we
241 imaged AtPIN1, SoPIN1 and PIN1b in the basal internode in mature plants 1cm above
242 the rosette. Here AtPIN1 normally accumulates in a highly polar manner in the rootward
243 plasma membranes of cambium (ca) and xylem parenchyma (xp) vascular-associated

244 tissues (Figure 3G, 3J) (Bennett et al., 2016; Gälweiler et al., 1998). PIN1b accumulated
245 in a similar pattern to AtPIN1 (Figure 3I, 3L. 10 samples from 5 events). In contrast, in
246 addition to accumulating in the cambium and xylem parenchyma, SoPIN1 accumulated
247 in the mature cortex (co) and central pith tissues (p) (Figure 3H, 3K. 15 samples from 4
248 events). AtPIN1 is not normally observed in the mature cortex or pith tissues (Figure 3G,
249 3J) (Bennett et al., 2016; Gälweiler et al., 1998). However we detected abundant
250 AtPIN1 expression in the immature pith closer to the apex (Figure 3D box, Figure 3 –
251 supplement 1 panel D) suggesting that *proAtPIN1* initially drives expression in a broad
252 domain and that AtPIN1 and PIN1b are both cleared from the cortex and pith by
253 maturity, while SoPIN1 is not. In the basal internode all three proteins showed the
254 characteristic rootward polarization pattern regardless of tissue-level abundance (Figure
255 3 – supplement 1 panels D, E, F arrows).

256 Taken together these results show that even under the same transcriptional control
257 AtPIN1, SoPIN1 and PIN1b show distinct tissue-level accumulation patterns in
258 Arabidopsis. While the overall behavior of the two Brachypodium proteins is similar to
259 AtPIN1 in many tissues, there are behaviors unique to each. PIN1b fails to accumulate
260 in epidermal tissues where AtPIN1 and SoPIN1 remain high, whereas SoPIN1
261 accumulates in the mature cortex and pith tissue where AtPIN1 and PIN1b do not. The
262 convergent polarization patterns of SoPIN1 and the vascular accumulation of PIN1b in
263 Arabidopsis are remarkably similar to their native behaviors in Brachypodium (O'Connor
264 et al., 2014) suggesting protein-intrinsic features might control tissue level accumulation
265 in the two species.

266

267 **SoPIN1 but not PIN1b can restore organ initiation and bulk auxin**
268 **transport in AtPIN1 null mutants**

269 To determine whether the observed differences in SoPIN1 and PIN1b polarization and
270 accumulation have functional consequences in Arabidopsis, we used the *proAtPIN1*-
271 driven SoPIN1 and PIN1b constructs to complement the Arabidopsis *pin1-613* mutant
272 (also known as *pin1-7)*. The *pin1-613* allele is a putative null T-DNA insertion allele with
273 severe organ initiation defects in the inflorescence (Absmanner et al., 2014; Bennett et
274 al., 2006; Smith et al., 2006). Given that epidermal AtPIN1 function is important for
275 organ initiation (Bilsborough et al., 2011; Kierzkowski et al., 2013), as expected only
276 SoPIN1 and not PIN1b was able to complement the *pin1-613* mutation and mediate
277 organ initiation (Figure 4A). 3 out of 6 independent SoPIN1-expressing transgenic
278 events showed complementation whereas all 10 independent PIN1b-expressing
279 transgenic events failed to complement. However phenotypic complementation of *pin1-*
280 *613* by SoPIN1 was incomplete with mature plants showing a variety of phenotypic
281 defects (Figure 4A, Figure 4 - supplement 1). Most notably each flower produced more
282 sepals and petals than wild-type but almost no stamens (Figure 4C, Figure 4 -
283 supplement 2). SoPIN1-complemented *pin1-613* plants were thus sterile. We wondered
284 whether these phenotypes could be explained by poor auxin transport function of
285 SoPIN1 in Arabidopsis. However SoPIN1 restored wild-type levels of bulk auxin
286 transport to *pin1-613* basal internodes (Figure 4D). Thus SoPIN1 is capable of
287 supporting organ initiation and mediating rootward auxin transport in the stem, but it is
288 not functionally identical to AtPIN1 expressed under the same promoter.

289 In SoPIN1-complemented *pin1-613* mutants, SoPIN1 protein accumulation in the
290 meristem epidermis was higher than that observed in a wild-type or heterozygous
291 genetic background and the pronounced convergent polarization patterns observed in
292 the wild-type background were less defined (Figure 5A, Figure 5 - supplement 1) (16 of
293 16 meristems). SoPIN1-complemented meristems showed a variety of phyllotactic
294 defects and had highly variable morphologies (Figure 5 – supplement 1 panel B) (16 of
295 16 meristems). Similar to the pattern observed in the wild-type background, sub-
296 epidermal SoPIN1 in *pin1-613* mutants accumulated in a loosely defined ring within
297 which individual vein traces were difficult to discern (Figure 5I) (13 of 16 meristems). In
298 mature tissues SoPIN1 accumulated in the epidermis, vasculature and pith, similar to
299 the wild-type background (Figure 5C, 5E, 5G).

300 In contrast to SoPIN1, PIN1b-expressing *pin1-613* plants had pin-formed inflorescences
301 that were indistinguishable from *pin1-613* alone (Figure 4A) (all 10 expressing events
302 failed to complement). The lack of complementation mediated by PIN1b was not caused
303 by silencing or low expression level because abundant PIN1b signal was observed in
304 *pin1-613* meristems (23 of 26 *pin1-613* meristems from 7 events). In contrast to the
305 wild-type background, most PIN1b expressing *pin1-613* samples had abundant
306 epidermal expression forming a ring-shaped domain around the meristem apex (Figure
307 5B, 5D arrow, Figure 5 - supplement 2) (14 of 19 meristems from 6 events). Also unlike
308 the wild-type background, PIN1b in the epidermis of *pin1-613* meristems was more
309 consistently targeted to the membrane and was often polar (Figure 5K). However even
310 with this elevated polar expression in the meristem epidermis, PIN1b was unable to
311 mediate organ initiation in *pin1-613* mutants. Below the apex PIN1b was polarized

312 rootward in *pin1-613* meristems (Figure 5J), forming defined traces associated with the
313 vasculature (Figure 5F, 5L). In the basal stem of *pin1-613* mutants PIN1b accumulated
314 in a pattern similar to wild-type, although the arrangement of vascular bundles was
315 irregular (Figure 5H). Remarkably, despite clear polar PIN1b expression in *pin1-613*
316 mutant stems (Figure 5M), PIN1b was unable to rescue bulk auxin transport in this
317 tissue (Figure 4D).

318 Because PIN1b seemed to form more defined sub-epidermal traces than SoPIN1
319 (Compare Figure 3 – supplement 1 panels B and C, and Figure 5I and 5L) we thought
320 PIN1b combined with SoPIN1 may improve the partial SoPIN1-mediated
321 complementation of *pin1-613*. We tested two independent PIN1b events for
322 complementation of *pin1-613* when combined with a SoPIN1 event that showed partial
323 complementation, but all double SoPIN1/PIN1b expressing *pin1-613* plants appeared
324 phenotypically similar to the SoPIN1-only complementation (data not shown). Thus
325 SoPIN1 combined with PIN1b is no better than SoPIN1 alone. In total these results
326 demonstrate that when expressed in *Arabidopsis,* there is a clear functional separation
327 between SoPIN1 and PIN1b independent of transcriptional control.

328

329 SoPIN1 and PIN1b show different behaviors when expressed in the 330 meristem epidermis

331 Epidermal-specific AtPIN1 expression is sufficient to rescue organ initiation in *atpin1*
332 mutants (Bilsborough et al., 2011), highlighting the importance of AtPIN1 epidermal
333 expression to organ initiation. We wanted to test specifically the ability of SoPIN1 and

334 PIN1b to perform this epidermal function. In order to drive increased PIN1b expression
335 in the epidermis and to help reduce transgene position-effect variation of expression
336 level, we utilized a two-component expression system in the Landsberg *erecta* (L*er*)
337 background to drive SoPIN1 and PIN1b under the control of the epidermis-enriched
338 Arabidopsis ML1 promoter (Hereafter designated *proAtML1*>>) (Lenhard and Laux,
339 2003; Sessions et al., 2002). Under the control of *proAtML1* we achieved consistently
340 high epidermal accumulation of both SoPIN1 and PIN1b, but similar to the *proAtPIN1*
341 driven expression described above, only SoPIN1 showed clear convergent polarization
342 patterns around the sites of organ initiation (Figure 6A-6D, Figure 6 supplement 1 and
343 2) (11 of 11 meristems from 2 events). Despite consistently high epidermal expression
344 with this system, PIN1b polarity remained difficult to determine and in many cells the
345 abundance of protein on the membrane remained low (Figure 6D) (13 of 13 meristems
346 from 2 events). Instead PIN1b accumulated in intracellular bodies, especially in the cells
347 of the apical dome and the central domain of initiating organs (Figure 6 – supplement 3
348 panels A-D). Intracellular PIN1b did not co-localize with early endosomes as assayed by
349 FM4-64 (Figure 6 – supplement 3 panel C arrows), or show the perinuclear localization
350 characteristic of the endoplasmic reticulum, suggesting accumulation in either the golgi
351 apparatus or in vacuoles. PIN1b abundance and polarity was highest at the boundaries
352 of lateral organs (Figure 6 - supplement 2). Thus SoPIN1 and PIN1b show consistent
353 behaviors in the meristem epidermis when expressed under either *proAtPIN1* or
354 *proAtML1.* Despite increased PIN1b expression under *proAtML1* and a resulting
355 increase in protein accumulation in the apex, PIN1b was still unable to form convergent
356 polarization patterns in wild-type plants.

357 **Both SoPIN1 and PIN1b can rescue the Arabidopsis *pin1-4* mutation**
358 **when expressed in the meristem epidermis**

359 In order to determine whether the increased PIN1b abundance in the epidermis
360 achieved by the *proAtML1* two-component system had functional consequences, we
361 crossed these transgenes to the *pin1-4* mutant allele. The *pin1-4* allele is in the
362 Landsberg *erecta* (L*er*) background and has a single P579 to L amino acid change in
363 the second-to-last transmembrane domain of AtPIN1 (Bennett et al., 1995), but the
364 phenotype is similarly severe to the null *pin1-613* allele (Figure 7A-C). However using
365 immuno-localization we detected abundant AtPIN1 protein produced in *pin1-4*
366 meristems (Figure 7C), while similar to previous authors we did not detect any protein in
367 pin meristems of the null *pin1-613* allele (Figure 7B) (Absmanner et al., 2014; Bennett et
368 al., 2006) (6 *pin1-613* meristems, 5 *pin1-4* meristems). The AtPIN1 protein detected in
369 *pin1-4* mutants accumulated primarily in the provascular tissues below the pin apex
370 (Figure 7C) and appeared apolar (Figure 7D). Instead the perinuclear AtPIN1
371 localization in *pin1-4* suggests accumulation in the endoplasmic reticulum (Figure 7D,
372 arrow). The presence of AtPIN1 protein produced in *pin1-4* mutants indicates that
373 *AtPIN1* in this background may retain partial function despite the severity of the mutant
374 phenotype.

375 Indeed both SoPIN1 and PIN1b driven by *proAtML1* were able to rescue the organ
376 formation defects of *pin1-4* (Figure 8A). In contrast to the partial SoPIN1-mediated
377 complementation and failure of PIN1b to complement *pin1-613* described above, both
378 SoPIN1 and PIN1b-complemented *pin1-4* plants made WT flowers that produced seed

379 (Figure 8 – supplement 1). In addition SoPIN1 and PIN1b were both able to rescue bulk
380 auxin transport in the *pin1-4* basal internode, although PIN1b was less effective than
381 SoPIN1 (Figure 8B). In general SoPIN1 and PIN1b-mediated complementation of *pin1-4*
382 was phenotypically similar, but perhaps as a result of the decreased transport rate in
383 PIN1b-complemented *pin1-4* plants, this genotype showed a significant increase in
384 stem diameter (Figure 8C), providing further evidence that SoPIN1 and PIN1b are not
385 functionally equal.

386 SoPIN1-complemented *pin1-4* meristems were slightly smaller than wild-type (Figure 6
387 – supplement 1), but the protein localization was similar to the pattern observed in the
388 WT background, with clear convergent polarization around initiating organs (Figure 6E,
389 6G) (10 of 10 meristems from 1 event). In contrast, compared to the WT background,
390 PIN1b localization in *pin1-4* was dramatically altered (compare Figure 6B with Figure
391 6F). Most obvious was an increase in membrane targeted PIN1b and a corresponding
392 reduction in intracellular PIN1b (Figure 6H, Figure 6 supplement 3 panels E-H). PIN1b
393 polarization in the *pin1-4* background was more apparent than in wild-type, and
394 convergent polarization patterns clearly marked incipient organs (Figure 6H) (10 of 10
395 meristems from 1 event). PIN1b-complemented meristems accumulated less PIN
396 protein in the apical dome compared to SoPIN1-complemented meristems, and the
397 meristems were larger (Figure 6 – supplement 2).

398 In the basal internode, both PINs had similar accumulation patterns in the cortex (co)
399 and epidermis layers (Figure 6I-J arrows) and both showed rootward polarization in the
400 epidermis (Figure 6K-L arrows). Despite this expression domain being drastically
401 different than the wild-type vascular-associated pattern of AtPIN1 (Bennett et al., 2006;

402 Gälweiler et al., 1998), expression in these few cortex layers and epidermis was
403 apparently sufficient to drive near wild-type levels of rootward bulk auxin transport in
404 *pin1-4* (Figure 8B). Thus while both proteins can complement the *pin1-4* organ initiation
405 phenotype, the SoPIN1 and PIN1b complemented lines have differing localization
406 patterns, slightly different auxin transport properties and minor differences in meristem
407 and mature plant morphologies, suggesting once again that SoPIN1 and PIN1b are not
408 functionally identical.

409

410 # Discussion

411 ## The SoPIN1 and PIN1 clades have different functions in
412 ## Brachypodium

413 During spikelet development in Brachypodium, SoPIN1 forms convergent polarization
414 patterns surrounding the sites of organ initiation and strong expression of the auxin
415 response reporter DR5 (O'Connor et al., 2014). We provide additional evidence here
416 that SoPIN1 polarizes towards sites of high auxin concentration by showing that a DII
417 minimum occurs at SoPIN1 convergence points. In *sopin1* mutants the reduction of DII
418 does not occur, suggesting that SoPIN1 functions to concentrate auxin at epidermal
419 maxima, and similar to Arabidopsis, this is required for organ initiation in the
420 inflorescence. The barren inflorescence phenotype of *sopin1-1* mutants and the
421 specificity of SoPIN1 for the outer tissues and for convergent polarization patterns in
422 Brachypodium provides further support for the idea that auxin maximum formation is

423 necessary for organ initiation and that this is primarily mediated by convergent PIN in
424 the meristem epidermis (Bhatia et al., 2016; Jönsson et al., 2006; Kierzkowski et al.,
425 2013; Smith et al., 2006).

426 SoPIN1 clade mutants have been reported in the legume *Medicago truncatula* and in
427 tomato (*Solanum lycopersicum*) and these mutants show pleiotropic phenotypes
428 involving phyllotaxy, organ initiation, inflorescence branching, leaf serrations and leaf
429 compounding, but they do not form barren pin meristems (Martinez et al., 2016; Zhou et
430 al., 2011). These wider morphogenetic events also involve epidermal PIN convergence
431 points and associated auxin maxima (Barkoulas et al., 2008; Bilsborough et al., 2011),
432 suggesting a general role for SoPIN1 clade members in generating such maxima. The
433 lack of barren pin-formed meristems in these mutants suggests that different species
434 are variably dependent on SoPIN1-generated auxin maxima for organ initiation. Even in
435 Brachypodium and Arabidopsis, barren meristems in *sopin1* and at*pin1* respectively are
436 restricted to later stages of development, so organs are able to form in the absence of
437 SoPIN1 or AtPIN1 function.

438 In contrast to *sopin1* mutants, loss of *pin1* clade function in Brachypodium has very little
439 effect on organ initiation despite both PIN1a and PIN1b being expressed and polarized
440 away from auxin maxima in developing organs (O'Connor et al., 2014). Auxin drainage
441 is thought necessary for proper organ size and placement (Bhatia et al., 2016; Deb et
442 al., 2015) but the most evident phenotype in *pin1a/pin1b* mutants is the alteration of
443 internode length. The increased internode length in *pin1b* and severely reduced
444 internode length in *pin1a/pin1b* double mutants provides new genetic tractability to
445 address how PINs regulate tissue growth in the shoot independent of organ initiation, a

446 PIN function that is experimentally inaccessible in Arabidopsis because of the initiation
447 defects of *atpin1* mutants.

448 Grasses contain intercalary meristems, bands of indeterminate tissue separated from
449 the apical meristem that are responsible for internode growth after organ initiation.
450 Auxin dynamics in this more basal meristematic tissue may be important for controlling
451 stem growth. Indeed loss of the ABCB1 auxin exporter in maize and Sorghum results in
452 dwarfism associated with reduced activity of intercalary meristems (Knöller et al., 2010;
453 Multani et al., 2003). The role of PIN1a and PIN1b in regulating intercalary meristem
454 growth will be an important avenue for future work, especially since plant stature has
455 played such an important role in grass domestication.

456

457 The properties that define PIN behavior and function

458 **Membrane accumulation.** We used heterologous expression of SoPIN1 and PIN1b in
459 Arabidopsis to explore the ways in which different PIN family members may have
460 different properties post-transcription (Summarized in Figure 9). When expressed in the
461 meristem epidermis in wild-type Arabidopsis, SoPIN1 is localized to the membrane in
462 most cells while PIN1b often accumulates internally (Figure 6 - supplement 3). Thus
463 with the same transcriptional control, different PINs can vary in the degree to which,
464 after protein production, they accumulate at the plasma membrane. The differential
465 membrane targeting of PIN1b and SoPIN1 is a tissue-specific phenomenon however,
466 because unlike in the epidermis, in the basal internode both PINs accumulate at the
467 rootward plasma membrane (Figure 3 - supplement 1 panels E and F). The regulation

468 of PIN plasma membrane polar targeting and endocytic recycling has been an important
469 avenue for understanding PIN function and general membrane protein biology
470 (Luschnig and Vert, 2014). Our results provide further evidence that at least some of the
471 signals governing membrane accumulation are inherent in, and vary between, different
472 PIN family members (Wisniewska et al., 2006).

473 **Tissue accumulation.** Under the same transcriptional control AtPIN1, SoPIN1 and
474 PIN1b show different tissue-level accumulation patterns in Arabidopsis. In wild-type
475 plants, *proAtPIN1*-expressed PIN1b shows reduced overall accumulation in the
476 epidermis compared to AtPIN1 or SoPIN1 (Compare Figure 3D-3F). Even with greater
477 expression under *proAtML1,* the intracellular PIN1b signal observed in the meristem
478 epidermis (Figure 6 - supplement 3) suggests that PIN1b protein could be actively
479 targeted to the vacuole for degradation as has been shown for PIN2 in the root (Abas et
480 al., 2006; Kleine-Vehn et al., 2008b). In contrast, SoPIN1 is abundant in the meristem
481 epidermis and accumulates in the mature cortex and pith tissues where AtPIN1 and
482 PIN1b do not (Figure 3H arrows). Because we observed clear AtPIN1 accumulation in
483 the immature pith (Figure 3 - supplement 1 panel D), this suggests that *proAtPIN1* is at
484 least initially active in pith tissue and that the PIN1 clade members AtPIN1 and PIN1b
485 are removed later in development, while SoPIN1 is not. Laser capture micro-dissection
486 and RNAseq of mature stem tissue has detected abundant *AtPIN1* transcription in the
487 mature pith (T. Greb, personal communication, February 2017) suggesting that even at
488 maturity AtPIN1, and probably PIN1b, are actively cleared post-transcriptionally from
489 this tissue. Our results suggest that the AtPIN1 expression domain is far broader than is

490 indicated by the protein accumulation pattern and further highlight the importance of PIN
491 post-transcriptional regulation for controlling PIN tissue-level abundance.

492 In Arabidopsis endogenous PIN family members show a degree of cross-regulation
493 where loss-of-function mutations in one PIN family member result in tissue-level
494 accumulation of a different PIN in a compensatory pattern (Blilou et al., 2005; Paponov
495 et al., 2005; Vieten et al., 2005). We observed similar behavior in the *pin1-613* null
496 background where SoPIN1 and PIN1b accumulation in the meristem epidermis was
497 increased in the absence of AtPIN1 (Figure 5 supplements 1 and 2). This sensitivity of
498 SoPIN1 and PIN1b to the presence of AtPIN1, even while under the *AtPIN1* promoter,
499 suggests that wild-type AtPIN1 is able to compete with SoPIN1 and PIN1b post-
500 transcriptionally for residency at the membrane. However we did not observe the same
501 competitive effect with *proAtML1* where SoPIN1 and PIN1b tissue-level accumulation,
502 though not membrane residence, seemed similar between *pin1-4* mutant and wild-type
503 meristems (Figure 6 - supplements 1 and 2). This difference between *proAtPIN1* and
504 *proAtML1* may be because PIN transcription under *proAtPIN1* is sensitive to the dosage
505 of other PINs as has been suggested (Vieten et al., 2005). Alternatively, the lack of
506 increased SoPIN1 and PIN1b accumulation in the *pin1-4* mutant background may be
507 because the AtPIN1 protein produced in *pin1-4* is still able to compete with the other
508 expressed PINs. Regardless, these results highlight the sensitivity of PIN tissue-level
509 abundance to both transcriptional and post-transcriptional control, and the variability
510 between PIN family members independent of transcription.

511 **Transport activity.** In Arabidopsis phosphorylation of PINs by several different families
512 of protein kinases is thought necessary for efficient auxin transport (Absmanner et al.,

513 2014; Barbosa et al., 2014; Jia et al., 2016; Willige et al., 2013). PIN activation by
514 phosphorylation may explain the inability of PIN1b to mediate bulk auxin transport in the
515 basal internode of *pin1-613* plants despite being expressed, accumulating at the
516 membrane and being polarized rootward in this tissue (Figure 4D, Figure 5M). It is
517 possible that in the *proAtPIN1* domain PIN1b does not interact with the appropriate
518 activating kinase and it is thus unphosphorylated and inactive. Indeed a partially
519 unphosphorylatable form of AtPIN1 fails to complement fully the bulk auxin transport
520 defect of *pin1-613* mutants in the basal internode (Absmanner et al., 2014) and AtPIN1
521 polarity can be uncoupled from phosphorylation status, and thus presumably transport
522 activity can be independent of polarization (Weller et al., 2017).

523 However, when expressed using *proAtML1,* PIN1b expression in the outer tissue layers
524 of the basal internode appears sufficient to mediate bulk auxin transport in *pin1-4*
525 (Figure 8B). One explanation for this is that PIN1b activity may be tissue dependent,
526 perhaps because of the differing expression domains of activating kinases (Absmanner
527 et al., 2014). Arabidopsis PIN4 and PIN7 are present in the *proAtML1* domain (Bennett
528 et al., 2016) making it conceivable that these PINs are the normal targets of activating
529 kinases in this tissue. Alternatively, kinases in the L*er* genetic background may be more
530 effective at activating PIN1b than those in Col, but the dramatic effect of the *pin1-4*
531 allele vs wild-type *AtPIN1* on PIN1b polarization behavior within the L*er* background
532 makes this explanation unlikely (see below). In either case the behavior of PIN1b in
533 *pin1-613* provides a clear indication that even once a PIN has accumulated at the cell
534 membrane in a tissue it may not be active.

535 **Interaction.** A particularly striking result is the ability of PIN1b to form convergent
536 polarization patterns and mediate organ initiation in the *pin1-4* missense mutant
537 background when it is unable to do so in the null *pin1-613* background. It is unlikely that
538 differences between *proAtPIN1* and *proAtML1*-mediated expression can explain this
539 differential complementation because both promoters drive expression in the epidermis
540 and both promoters are sufficient to complement *atpin1* mutants using wild-type AtPIN1
541 as well as SoPIN1. As described above, it is possible that differences in activating
542 enzymes or similar interactors between the L*er* and Col backgrounds could contribute to
543 the strikingly different behavior of PIN1b in *pin1-4* vs *pin1-613*. Indeed mutation of the
544 leucine-rich repeat receptor-like kinase *ERECTA,* which is mutated in the L*er*
545 background, has known effects on PIN1 localization when combined with other
546 mutations in the *ERECTA* family (Chen et al., 2013; Torii et al., 1996). However the
547 dramatic effect of wild-type AtPIN1 vs *pin1-4* on PIN1b membrane targeting (compare
548 Figure 6 - supplement 3 panels A-D to E-H) within the L*er* background suggests the
549 differing genetic backgrounds of each complementation (L*er* vs Col-0) is not sufficient to
550 explain the differential complementation.

551 Instead the strong influence of *pin1-4* on PIN1b membrane targeting and polarity in the
552 meristem epidermis suggests that PIN1b may be cooperating with a partially functional
553 *pin1-4* protein and together they recapitulate the organ initiation functions of wild-type
554 AtPIN1. PIN1b interaction with *pin1-4* in the outer cortex of the stem may also explain
555 the ability of PIN1b to rescue bulk transport in the basal internodes of *pin1-4* mutants
556 while it cannot in the null *pin1-613* allele. Partial *pin1-4* function is further supported by
557 the result that SoPIN1 complementation of the null *pin1-613* allele is incomplete and

558 because of flower defects the plants are sterile (Figure 4C), while SoPIN1-mediated
559 complementation of *pin1-4* is complete and flowers are phenotypically normal and set
560 seed (Figure 8 - supplement 1). Accordingly SoPIN1 convergent polarization patterns
561 are more evident in the presence of *pin1-4* than they are during complementation of the
562 null *pin1-613* allele (Compare 5A and 6E), further evidence that residual *pin1-4* function
563 augments SoPIN1 during *pin1-4* complementation. Combined these data suggest that
564 the *pin1-4* allele is hypomorphic and that it provides some necessary function to PIN1b.

565 If PIN1b is indeed inactive in null *pin1-613* mutants as we hypothesized above then it is
566 possible *pin1-4* facilitates the interaction of PIN1b with the appropriate activating kinase
567 and this allows PIN1b to perform organ initiation and bulk transport. Alternatively
568 interaction between PIN1b and *pin1-4* may facilitate proper membrane targeting or
569 polarization of either protein, resulting in functional transport. The increased level of
570 polar, plasma-membrane localized PIN1b in *pin1-4* meristems supports the idea that
571 *pin1-4* controls PIN1b membrane residency, but it cannot explain why PIN1b appears
572 unable to mediate bulk transport in *pin1-613* despite being membrane-localized and
573 polar in the basal internode.

574 Direct PIN-PIN interactions have so far not been shown, but if one PIN type can convey
575 targeting, polarity or activity information to another through direct or indirect interaction,
576 this may be relevant to auxin transport in tissues where multiple PINs are coexpressed,
577 such as in the Arabidopsis root meristem (Blilou et al., 2005), or in the shoot apical
578 meristems of most angiosperms where the SoPIN1 and PIN1 clade proteins likely
579 overlap, as they do during spikelet development in Brachypodium (O'Connor et al.,
580 2014).

581 **Polarity.** We previously showed that the polarization dynamics of SoPIN1, PIN1a and
582 PIN1b in *Brachypodium* could be modeled by assigning two different polarization modes
583 to the SoPIN1 and PIN1 clades (O'Connor et al., 2014). In the model, SoPIN1 orients
584 toward the adjacent cell with the highest auxin concentration thus transporting auxin up
585 the concentration gradient and providing a positive feedback to concentrate auxin into
586 local maxima. In contrast, in the model PIN1a and PIN1b proteins are allocated in
587 proportion to net auxin flux thus providing a positive feedback in which flux through the
588 tissue is amplified by the allocation of PIN1a/b in the direction of that flux. The
589 assignment of two different polarization modes was previously used to describe the
590 behavior of AtPIN1 during organ placement and vein patterning using an auxin-
591 concentration based switching mechanism between the up-the-gradient (UTG) and with-
592 the-flux (WTF) polarization modes (Bayer et al., 2009). However it has also been
593 suggested that a flux-based mechanism alone can account for both convergence points
594 and vein patterning (Abley et al., 2016; Cieslak et al., 2015; Stoma et al., 2008).

595 Despite evidence that convergent PIN polarization is dependent on localized auxin
596 signaling in adjacent cells (Bhatia et al., 2016), there are still no proven mechanisms for
597 direct sensing of intercellular auxin gradients or auxin fluxes across membranes. The
598 *sopin1, pin1a* and *pin1b* phenotypes in Brachypodium are consistent with different
599 polarization modes. SoPIN1 is required for organ initiation and the formation of auxin
600 maxima in Brachypodium, which is primarily modeled using UTG polarization (Bayer et
601 al., 2009; Jönsson et al., 2006; Smith et al., 2006). On the other hand, *pin1a* and *pin1b*
602 mutant plants do not show organ initiation defects, but rather only have internode
603 elongation defects, a tissue where WTF models have been used to explain PIN

604 dynamics and measured auxin transport kinetics during vein patterning and the
605 regulation of branch outgrowth (Bayer et al., 2009; Bennett et al., 2016; Mitchison,
606 1980; Mitchison et al., 1981; Prusinkiewicz et al., 2009).

607 In wild-type Brachypodium, the SoPIN1 and PIN1a/b expression domains are almost
608 entirely mutually exclusive (O'Connor et al., 2014), making it possible that the observed
609 polarization differences between the two clades are due to expression context or tissue-
610 level stability and not to functional differences between the proteins themselves. More
611 specifically, perhaps an UTG mechanism dominates the epidermis while a WTF
612 mechanism is utilized in the internal tissues and different PINs interact equally with
613 these context-dependent mechanisms. Our heterologous expression studies do not
614 exclusively support context-dependent or protein-dependent mechanisms for SoPIN1
615 and PIN1 polarization. It is clear that alone only SoPIN1 and AtPIN1 show the
616 convergent polarization patterns associated with UTG polarization, and alone only
617 SoPIN1 and AtPIN1 are thus able to mediate organ initiation, while PIN1b cannot. On
618 the other hand, all three PINs are capable of rootward polarization in the basal
619 internode tissue and PIN1b can be co-opted to convergent polarization at the meristem
620 epidermis in the presence of *pin1-4*. The results presented here do not demonstrate
621 whether within a single cell SoPIN1 and PIN1b would orient differently with respect to
622 auxin as might be expected for the dual polarization model (O'Connor et al., 2014).
623 However such context-independent polarization behavior was previously observed for
624 PIN1 and PIN2 in the root where both PINs can polarize in opposing directions within a
625 single cell type when expressed in the PIN2 domain (Kleine-Vehn et al., 2008a;
626 Wisniewska et al., 2006).

627 ## Outlook

628 In total our Brachypodium mutant phenotypes and heterologous expression results point
629 to multiple levels at which PIN family members can be functionally distinct. Differential
630 membrane targeting, tissue level accumulation, transport activity, indirect or direct
631 interaction and the resultant polarity may all contribute to the dynamics of PIN action
632 during plant development. In most flowering plants two PIN clades, SoPIN1 and PIN1,
633 with differing functions and differing transcriptional and post-transcriptional properties
634 mediate auxin transport in the shoot, but these properties are seemingly combined into
635 AtPIN1 in Arabidopsis and other Brassicaceae species. Because PIN1b alone is unable
636 to mediate organ initiation while AtPIN1 can, and these two PINs are both members of
637 the same clade, AtPIN1 may have gained the ability to form convergent polarization
638 patterns and mediate organ initiation after or coincident with the loss of the SoPIN1
639 clade. Indeed when comparing Brassicaceae PIN1 proteins against a broad sampling of
640 other angiosperm PIN1 proteins, the Brassicaceae PIN1 proteins have several
641 divergent protein domains (Figure 9 - supplement 1), suggesting possible
642 neofunctionalization within the Brassicacea family. Alternatively an expansion of the
643 PIN3,4,7 clade is also characteristic of Brassicacea species (Bennett et al., 2014;
644 O'Connor et al., 2014), making it possible duplicated members of this clade buffered the
645 loss of SoPIN1. However there is no indication that PIN3,4,7 have a role in organ
646 initiation in the inflorescence (Guenot et al., 2012). Regardless, we believe the
647 combination of SoPIN1 and PIN1 characteristics into AtPIN1 coincident with the loss of
648 the SoPIN1 clade represents a form of reverse-subfunctionalization, the combination of
649 functions originally split between homologs into a single protein after gene loss. It is not

650 surprising that PINs may be particularly amenable to this kind of functional evolution
651 because, as described above, there are several post-transcriptional regulatory steps
652 that ultimately combine to control PIN function in plants. The output of auxin transport is
653 the sum of an extensive network of post-transcriptional interactions that all act to
654 regulate auxin transport itself, and this gives the system plasticity during development
655 and perhaps also over evolutionary time.

656

657 Materials and Methods

658 *sopin1-1*, *pin1a-1,* and *pin1b-1* creation with CRISPR

659 SoPIN1 (Bradi4g26300), PIN1a (Bradi1g45020) and PIN1b (Bradi3g59520) were
660 targeted with CRISPR using vectors developed for rice (Miao et al., 2013). CRISPR
661 constructs were transformed into Brachypodium inbred line Bd21-3 using previously
662 published methods (Bragg et al., 2015).

663 *sopin1-1* CRISPR

664 The SoPIN1 guide was AGGCTGTCGTACGAGGAGT. This guide was shorter than the
665 typical 20bp in an effort to provide greater target specificity for SoPIN1 (Fu et al., 2014).
666 In the T0 regenerated plants 5 out of 9 independent transgenic events showed severe
667 organ initiation defects and all 5 contained lesions in the SoPIN1 CRIPSR target site.
668 Unfortunately only one of the events with a T0 phenotype set seed. In the T1 progeny of
669 this event only those individuals that contained the CRISPR transgene showed lesions

670 in the SoPIN1 CRISPR target site and these plants showed the *sopin1* phenotype and
671 thus failed to set seed, suggesting active editing by the SoPIN1 CRISPR transgene in
672 this event.

673 Not all events showed such efficient editing however, and we identified an independent
674 T1 family where a C insertion in the SoPIN1 CRISPR target site co-segregated with the
675 barren inflorescence phenotype. We designated this allele, which causes a premature
676 stop codon before the end of the third exon codon 739 base pairs downstream from the
677 target site, *sopin1-1*. (Primer IDs 1-2 Table 1) We backcrossed a heterozygous *sopin1-1*
678 plant to the Bd21-3 parental line and all F1 progeny (N=4) were wild-type. In the F2
679 generation, plants homozygous for the *sopin1-1* lesion co-segregated with the barren
680 inflorescence phenotype (N=60: 32 het, 18 homo,10 wt). Amongst these plants, 16 did
681 not have the Cas9 transgene (Primer IDs 3-4 Table 1) and the barren inflorescence
682 phenotype still co-segregated with the *sopin1-1* lesion (N=16: 8 het, 3 homo, 5 wt). We
683 crossed the T1 *sopin1-1* heterozygous plant with a line homozygous for the previously
684 published SoPIN1-CITRINE genomic reporter line (O'Connor et al., 2014). In the F2 we
685 identified two individuals homozygous for *sopin1-1* but heterozygous for the SoPIN1-
686 CITRINE transgene. Only F3 progeny individuals that lacked the SoPIN1-CITRINE
687 transgene showed a *sopin1-1* phenotype, while those that contained the SoPIN1-
688 CITRINE transgene made spikelets and set seed (N=34: 6 *sopin1-1* phenotype, 28 wt
689 phenotype) (Figure 1 - supplement 1). This complementation was independent of the
690 presence of Cas9.

691

692 *pin1a-1* CRISPR

693 The PIN1a guide was ATCTACTCCCGGCGGTCCAT. We identified edited plants in the
694 T1 generation (Primer IDs 5-6 Table 1), then found a homozygous T insertion in the T2
695 generation which was independent of Cas9, resulting in a premature stop codon 939
696 base pairs downstream, here designated *pin1a-1*. No single-mutant *pin1a-1* phenotypes
697 were observed.

698 *pin1b-1* CRISPR

699 The PIN1b guide was AGGGCAAGTACCAGATCC. We identified a single plant from
700 the regenerating T0 PIN1b CRISPR population that had longer basal internodes and
701 twisted leaves. This plant was homozygous for an A deletion in the PIN1b CRISPR
702 target site causing a premature stop in the second exon 502 base pairs downstream,
703 here designated *pin1b-1* (Primer IDs 7-8 Table 1). All T1 progeny showed the *pin1b*
704 phenotype and were homozygous for the *pin1b-1* lesion. We backcrossed these T1
705 plants to Bd21-3 and all F1 progeny had a wild-type phenotype (N=11). In the F2, the
706 *pin1b* phenotype co-segregated with the *pin1b-1* lesion (N= 215, 91 het, 39 homo, 26
707 wt). Amongst these plants, 24 did not have the Cas9 transgene and the *pin1b*
708 phenotype still co-segregated perfectly with the *pin1b-1* lesion (N=24: 10 het, 6 homo, 8
709 wt). We crossed *pin1b-1* without Cas9 to a line homozygous for the previously
710 published PIN1b-CITRINE transgene (O'Connor et al., 2014). In the F3 we identified
711 lines homozygous for both the transgene and *pin1b-1* and used these to quantify
712 internode lengths compared to *pin1b-1* (Figure 2 - supplement 1).

713

714 *pin1a-1 / pin1b-1* double mutant.

715 Homozygous *pin1b-1* lacking Cas9 was crossed to homozygous *pin1a-1* lacking Cas9.
716 In the F2 phenotypically *pin1b-1* plants that were also genotyped heterozygous for
717 *pin1a-1* were identified. In the homozygous *pin1b-1* F3 generation the double *pin1a-1 /*
718 *pin1b-1* mutant phenotype segregated perfectly with the *pin1a-1* lesion (N=2: 10 het, 5
719 homo, 8 wt). Double *pin1a-1 / pin1b-1* mutants were easily identified by phenotype and
720 produce seed.

721 Brachypodium Reporter Constructs

722 All constructs were cloned using Multi-site Gateway (Invitrogen) and were transformed
723 into Brachypodium Bd21-3 using previously published methods (Bragg et al., 2015). For
724 pZmUbi::DII-Venus, we first cloned the maize ubiquitin promoter into pDONR P4-P1R
725 (Primer IDs 9-10 Table 1) and this was subsequently recombined with pDONR 221
726 containing Arabidopsis DII and pDONR P2R-P3 containing VENUS-N7 (Brunoud et al.,
727 2012) into the Multi-site Gateway binary vector pH7m34GW
728 (http://gateway.psb.ugent.be/). In the T3 generation, degradation of DII-Venus in the
729 presence of auxin was validated by treating excised Brachypodium spikelet meristems
730 with 1 μM 1-naphthaleneacetic acid (NAA) or mock treatment in 70% ethanol, and
731 imaging every 30 min (Figure 1 –supplement 2).

732 For SoPIN1-Cerulean, the promoter plus 5' coding pDONR-P4-P1R and 3' coding plus
733 downstream pDONR-P2R-P3 fragments from (O'Connor et al., 2014) were used. Maize
734 codon-optimized Cerulean florescent protein, courtesy of David Jackson, was amplified

735 with 5x Ala linkers and cloned into pENTR/D-TOPO. These three fragments were then
736 recombined into pH7m34GW.

737 Arabidopsis Reporter Constructs

738 All constructs were cloned using Multi-site Gateway (Invitrogen) and transformed using
739 standard floral dip. For *proAtPIN1* complementation, a 3.5kb Arabidopsis PIN1 promoter
740 region was amplified from a genomic clone previously reported to complement the *pin1*
741 (Heisler et al., 2005) and cloned into Gateway vector pDONR P4-P1R (Primer IDs 11-
742 12 Table 1). For each Brachypodium PIN-CITRINE fusion construct, the entire PIN
743 coding region, including the CITRINE insertion, was amplified from the previously
744 published reporter constructs (O'Connor et al., 2014) and cloned into pENTR /D-TOPO
745 (Primer IDs 13-16 Table 1). The CITRINE fusion in each is located in a position known
746 to complement *pin1* mutations (Heisler et al., 2010; Wisniewska et al., 2006; Xu et al.,
747 2006). The *proAtPIN1* pDONR P4-P1R and PIN coding region pENTR/D-TOPO vectors
748 were then recombined into Gateway binary vector pH7m24GW
749 (http://gateway.psb.ugent.be/) and transformed by floral dip into both Col-0 and plants
750 heterozygous for *pin1-613* (also known as *pin1-7,* SALK_047613) (Bennett et al., 2006;
751 Smith et al., 2006). Complementation was assessed in the T3 generation, and all plants
752 were genotyped for both the *pin1-613* mutation (Primer IDs 17-19 Table 1) and for
753 presence of the PIN transgene (Primer IDs 20-22 Table 1).

754 For the *proAtML1* lines the PIN coding regions with CITRINE insertion pENTR /D-TOPO
755 Gateway vectors were recombined downstream of the two-component OP promoter in
756 vector pMoA34-OP (Moore et al., 1998) and then transformed into the *proAtML1* driver

757 line in the Landsberg *erecta* background (Lenhard and Laux, 2003). Lines homozygous
758 for both the *proAtML1* driver and OP::PIN were crossed to het *pin1-4* and
759 complementation was assessed in the F2 and F3 generations. All complemented plants
760 were genotyped for *pin1-4* (Primer IDs 23-24 Table 1), the Brachypodium PINs (Primer
761 IDs 20-22 Table 1) and the presence of the ML1 driver transgene (Primer IDs 25-26
762 Table 1).

763 Confocal and Scanning Electron Microscopy

764 All confocal images were captured on a Zeiss 780 laser scanning confocal using a W
765 Plan-Apochromat 20x or 63x magnification 1.0 numerical aperture objectives. Detection
766 wavelengths: 517-570nm for CITRINE-tagged PINs, 535-552 for DII-Venus, 463-509 for
767 SoPIN1-CERULEAN, 490-543 for AtPIN1-GFP, 691-753nm for FM4-64, 561-606nm for
768 Dylight 549, 631-717nm for Propidium Iodide and 646-726 for chlorophyll A auto-
769 fluorescence. The pinhole was set to 1 airy unit for all meristem stacks and details of
770 sub-epidermal polarization but was open to the maximum setting for tiled longitudinal
771 and cross sections of the basal internode (Figures 3D-L, 5C-H and 6I-J). Detection gain
772 and laser power were varied according to signal strength unless direct comparisons
773 between genotypes were made as indicated in figure legends, except for Figure 1J and
774 1K where the DII gain was higher in Figure 1K in order to show DII distribution.

775 Cryo scanning electron microscopy was performed on a Zeiss EVO HD15 SEM fitted
776 with a LaB6 filament and a Quorum PP3010T (Quorum Technololgies, Lewes, Sussex.
777 UK) cryo preparation unit using the BSD (Backscattered electron) detector with probe

778 current as set to 10 nA, and 15.00 kV gun voltage. Frozen samples were coated in
779 <1.5nm Pt.

780 Auxin Transport Assays

781 Auxin transport assays were carried out as described in (Crawford et al., 2010). Briefly,
782 17 mm long basal internodes were excised and the apical end submerged in 30 µl
783 Arabidopsis salts (ATS) without sucrose (pH = 5.6) containing 1 µM ^{14}C-IAA (American
784 Radiolabeled Chemicals). After 6 hours incubation the basal 5 mm segment was
785 excised, cut in half, and shaken overnight at 400 RPM in 200 µl scintillation liquid prior
786 to scintillation counting. 10µM N-1-Naphthylphthalamic Acid (NPA), an auxin transport
787 inhibitor, was added prior to incubation for negative controls.

788 AtPIN1 Immuno-Localization

789 Detection of AtPIN1 in sectioned apexes was performed as previously described
790 (O'Connor et al., 2014). Commercial polyclonal goat anti-AtPIN1 (AP-20) was used at a
791 concentration of 1:150 (Santa Cruz Biotechnology). Affinity-purified Donkey Anti-Goat
792 Dylight 549 secondary was used at a concentration of 1:200 (Jackson Immuno
793 Research). Control samples where the primary antibody was omitted showed a similar
794 level of background signal as *pin1-613* null mutant samples.

795

796

797

Acknowledgments

Thanks to Raymond Wightman for SEM assistance, Martin van Rongen for assistance with transport assays and *pin1-613* oligos, Tom Bennett for *proAtPIN1* oligos, Marcus Heisler for AtPIN1-GFP construct and *pin1-4* genotyping assistance, Teva Vernoux for DII plasmids, David Jackson for maize codon-optimized Cerulean and to all the members of the Leyser lab. Thanks also to Graeme Mitchison, Katie Abley, Michael Raissig, and Pau Formosa-Jordan for helpful comments on the manuscript.

Competing interests

The authors have no competing interests.

References

Abas, L., Benjamins, R., Malenica, N., Paciorek, T., Wisniewska, J., Wirniewska, J., Moulinier-Anzola, J. C., Sieberer, T., Friml, J. and Luschnig, C. (2006). Intracellular trafficking and proteolysis of the Arabidopsis auxin-efflux facilitator PIN2 are involved in root gravitropism. *Nat Cell Biol* **8**, 249–256.

Abley, K., Marée, A. F. and Coen, E. (2016). Formation of polarity convergences underlying shoot outgrowths. *eLife* **5**, 2061.

Absmanner, B., Barbosa, I. C. R., Willige, B. C., Fastner, A., Streit, V., Port, S. A. and la Fuente van Bentem, de, S. (2014). Auxin efflux by PIN-FORMED proteins is activated by two different protein kinases, D6 PROTEIN KINASE and PINOID. *eLife* **3**.

Adamowski, M. and Friml, J. (2015). PIN-Dependent Auxin Transport: Action,

822 Regulation, and Evolution. *The Plant Cell* **27**, 20–32.

823 **Barbosa, I. C. R., Zourelidou, M., Willige, B. C., Weller, B. and**
824 **Schwechheimer, C.** (2014). D6 PROTEIN KINASE activates auxin transport-
825 dependent growth and PIN-FORMED phosphorylation at the plasma
826 membrane. *Dev Cell* **29**, 674–685.

827 **Barkoulas, M., Hay, A., Kougioumoutzi, E. and Tsiantis, M.** (2008). A
828 developmental framework for dissected leaf formation in the Arabidopsis
829 relative Cardamine hirsuta. *Nat Genet* **40**, 1136–1141.

830 **Bayer, E. M., Bayer, E. M., Smith, R. S., Mandel, T., Nakayama, N., Sauer, M.,**
831 **Prusinkiewicz, P. and Kuhlemeier, C.** (2009). Integration of transport-based
832 models for phyllotaxis and midvein formation. *Genes Dev* **23**, 373–384.

833 **Benková, E., Michniewicz, M., Sauer, M., Teichmann, T., Seifertová, D.,**
834 **Jürgens, G. and Friml, J.** (2003). Local, Efflux-Dependent Auxin Gradients
835 as a Common Module for Plant Organ Formation. *Cell* **115**, 591–602.

836 **Bennett, S. R. M., Alvarez, J., Bossinger, G. and Smyth, D. R.** (1995).
837 Morphogenesis in pinoid mutants of Arabidopsis thaliana. *Plant J* **8**, 505–520.

838 **Bennett, T. A., Brockington, S. F., Rothfels, C., Graham, S. W., Stevenson,**
839 **D., Kutchan, T., Rolf, M., Thomas, P., Wong, G. K.-S., Leyser, H. M. O., et**
840 **al.** (2014). Paralogous radiations of PIN proteins with multiple origins of
841 noncanonical PIN structure. *Molecular Biology and Evolution* **31**, 2042–2060.

842 **Bennett, T. A., Hines, G., van Rongen, M., Waldie, T., Sawchuk, M. G.,**
843 **Scarpella, E., Ljung, K. and Leyser, H. M. O.** (2016). Connective Auxin
844 Transport in the Shoot Facilitates Communication between Shoot Apices.
845 *PLoS Biol* **14**, e1002446.

846 **Bennett, T. A., Sieberer, T., Willett, B., Booker, J., Luschnig, C. and Leyser,**
847 **H. M. O.** (2006). The Arabidopsis MAX Pathway Controls Shoot Branching by
848 Regulating Auxin Transport. *Current Biology* **16**, 553–563.

849 **Bhatia, N., Bozorg, B., Larsson, A., Ohno, C., Jönsson, H. and Heisler, M. G.**
850 (2016). Auxin Acts through MONOPTEROS to Regulate Plant Cell Polarity
851 and Pattern Phyllotaxis. *Curr Biol* **26**, 3202–3208.

852 **Bilsborough, G. D., Runions, A., Barkoulas, M., Jenkins, H. W., Hasson, A.,**
853 **Galinha, C., Laufs, P., Hay, A., Prusinkiewicz, P. and Tsiantis, M.** (2011).
854 Model for the regulation of Arabidopsis thaliana leaf margin development.
855 *Proc Natl Acad Sci USA* **108**, 3424–3429.

856 **Blilou, I., Xu, J., Wildwater, M., Willemsen, V., Paponov, I., Friml, J., Heidstra,**
857 **R., Aida, M., Palme, K. and Scheres, B.** (2005). The PIN auxin efflux
858 facilitator network controls growth and patterning in Arabidopsis roots. *Nature*
859 **433**, 39–44.

860 **Bragg, J. N., Anderton, A., Nieu, R. and Vogel, J. P.** (2015). Brachypodium
861 distachyon. *Methods Mol Biol* **1223**, 17–33.

862 **Brunoud, G., Wells, D. M., Oliva, M., Larrieu, A., Mirabet, V., Burrow, A. H.,**
863 **Beeckman, T., Kepinski, S., Traas, J., Bennett, M. J., et al.** (2012). A novel
864 sensor to map auxin response and distribution at high spatio-temporal
865 resolution. *Nature* **482**, 103–106.

866 **Chen, M.-K., Wilson, R. L., Palme, K., Ditengou, F. A. and Shpak, E. D.**
867 (2013). ERECTA family genes regulate auxin transport in the shoot apical
868 meristem and forming leaf primordia. *Plant Physiol* **162**, 1978–1991.

869 **Cieslak, M., Runions, A. and Prusinkiewicz, P.** (2015). Auxin-driven patterning
870 with unidirectional fluxes. *J Exp Bot* **66**, 5083–5102.

871 **Crawford, S., Shinohara, N., Sieberer, T., Williamson, L., George, G.,**
872 **Hepworth, J., Muller, D., Domagalska, M. A. and Leyser, H. M. O.** (2010).
873 Strigolactones enhance competition between shoot branches by dampening
874 auxin transport. *Development* **137**, 2905–2913.

875 **Deb, Y., Marti, D., Frenz, M., Kuhlemeier, C. and Reinhardt, D.** (2015).
876 Phyllotaxis involves auxin drainage through leaf primordia. *Development* **142**,
877 dev.121244–2001.

878 **Derbyshire, P. and Byrne, M. E.** (2013). MORE SPIKELETS1 is required for
879 spikelet fate in the inflorescence of Brachypodium. *Plant Physiol* **161**, 1291–
880 1302.

881 **Fu, Y., Sander, J. D., Reyon, D., Cascio, V. M. and Joung, J. K.** (2014).
882 Improving CRISPR-Cas nuclease specificity using truncated guide RNAs. *Nat*
883 *Biotechnol* **32**, 279–284.

884 **Gälweiler, L., Guan, C., Müller, A., Wisman, E., Mendgen, K., Yephremov, A.**
885 **and Palme, K.** (1998). Regulation of Polar Auxin Transport by AtPIN1 in
886 Arabidopsis Vascular Tissue. *Science* **282**, 2226–2230.

887 **Gordon, S. P., Heisler, M. G., Reddy, G. V., Ohno, C., Das, P. and**
888 **Meyerowitz, E. M.** (2007). Pattern formation during de novo assembly of the
889 Arabidopsis shoot meristem. *Development* **134**, 3539–3548.

890 **Guenot, B., Bayer, E. M., Bayer, E., Kierzkowski, D., Smith, R. S., Mandel, T.,**
891 **Zádníková, P., Benková, E. and Kuhlemeier, C.** (2012). Pin1-independent
892 leaf initiation in Arabidopsis. *Plant Physiol* **159**, 1501–1510.

893 **Habets, M. E. J. and Offringa, R.** (2014). PIN-driven polar auxin transport in
894 plant developmental plasticity: a key target for environmental and
895 endogenous signals. *New Phytologist* **203**, 362–377.

896 **Heisler, M. G., Hamant, O., Krupinski, P., Uyttewaal, M., Ohno, C., Jönsson,**
897 **H., Traas, J. and Meyerowitz, E. M.** (2010). Alignment between PIN1 polarity
898 and microtubule orientation in the shoot apical meristem reveals a tight
899 coupling between morphogenesis and auxin transport. *PLoS Biol* **8**,
900 e1000516.

901 **Heisler, M. G., Ohno, C., Das, P., Sieber, P., Reddy, G. V., Long, J. A. and**
902 **Meyerowitz, E. M.** (2005). Patterns of auxin transport and gene expression
903 during primordium development revealed by live imaging of the Arabidopsis
904 inflorescence meristem. *Curr Biol* **15**, 1899–1911.

905 **Jia, W., Li, B., Li, S., Liang, Y., Wu, X., Ma, M., Wang, J., Gao, J., Cai, Y.,**
906 **Zhang, Y., et al.** (2016). Mitogen-Activated Protein Kinase Cascade MKK7-
907 MPK6 Plays Important Roles in Plant Development and Regulates Shoot
908 Branching by Phosphorylating PIN1 in Arabidopsis. *PLoS Biol* **14**, e1002550.

909 **Jönsson, H., Heisler, M. G., Shapiro, B. E., Meyerowitz, E. M. and Mjolsness,**
910 **E.** (2006). An auxin-driven polarized transport model for phyllotaxis. *Proc Natl*
911 *Acad Sci USA* **103**, 1633–1638.

912 **Kierzkowski, D., Lenhard, M., Smith, R. S. and Kuhlemeier, C.** (2013).
913 Interaction between meristem tissue layers controls phyllotaxis. *Dev Cell* **26**,
914 616–628.

915 **Kleine-Vehn, J., Dhonukshe, P., Sauer, M., Brewer, P. B., Wisniewska, J.,**
916 **Paciorek, T., Benková, E. and Friml, J.** (2008a). ARF GEF-dependent
917 transcytosis and polar delivery of PIN auxin carriers in Arabidopsis. *Curr Biol*
918 **18**, 526–531.

919 **Kleine-Vehn, J., Leitner, J., Zwiewka, M., Sauer, M., Abas, L., Luschnig, C.**
920 **and Friml, J.** (2008b). Differential degradation of PIN2 auxin efflux carrier by
921 retromer-dependent vacuolar targeting. *Proc Natl Acad Sci USA* **105**, 17812–
922 17817.

923 **Knöller, A. S., Blakeslee, J. J., Richards, E. L., Peer, W. A. and Murphy, A. S.**
924 (2010). Brachytic2/ZmABCB1 functions in IAA export from intercalary
925 meristems. *J Exp Bot* **61**, 3689–3696.

926 **Lenhard, M. and Laux, T.** (2003). Stem cell homeostasis in the Arabidopsis
927 shoot meristem is regulated by intercellular movement of CLAVATA3 and its
928 sequestration by CLAVATA1. *Development* **130**, 3163–3173.

929 **Leyser, H. M. O.** (2005). Auxin Distribution and Plant Pattern Formation: How
930 Many Angels Can Dance on the Point of PIN? *Cell* **121**, 819–822.

931 **Leyser, H. M. O.** (2006). Dynamic integration of auxin transport and signalling.
932 *CURBIO* **16**, R424–33.

933 **Leyser, H. M. O.** (2010). The power of auxin in plants. *Plant Physiol* **154**, 501–
934 505.

935 **Luschnig, C. and Vert, G.** (2014). The dynamics of plant plasma membrane
936 proteins: PINs and beyond. *Development* **141**, 2924–2938.

937 **Martinez, C. C., Koenig, D., Chitwood, D. H. and Sinha, N. R.** (2016). A sister
938 of PIN1 gene in tomato (Solanum lycopersicum) defines leaf and flower organ
939 initiation patterns by maintaining epidermal auxin flux. *Dev Biol* **419**, 85–98.

940 **Miao, J., Guo, D., Zhang, J., Huang, Q., Qin, G., Zhang, X., Wan, J., Gu, H.**
941 **and Qu, L.-J.** (2013). Targeted mutagenesis in rice using CRISPR-Cas
942 system. *Cell Res* **23**, 1233–1236.

943 **Mitchison, G. J.** (1980). A Model for Vein Formation in Higher Plants. *Proc. Biol.*
944 *Sci.* **207**, 79–109.

945 **Mitchison, G. J., Hanke, D. E. and Sheldrake, A. R.** (1981). The Polar
946 Transport of Auxin and Vein Patterns in Plants [and Discussion].
947 *Philosophical Transactions of the Royal Society B: Biological Sciences* **295**,
948 461–471.

949 **Moore, I., Gälweiler, L., Grosskopf, D. and Palme, K.** (1998). A transcription
950 activation system for regulated gene expression in transgenic plants. *Proc.*
951 *Natl. Acad. Sci. U.S.A.* **95**, 376–381.

952 **Multani, D. S., Briggs, S. P., Chamberlin, M. A., Blakeslee, J. J., Murphy, A.**
953 **S. and Johal, G. S.** (2003). Loss of an MDR transporter in compact stalks of
954 maize br2 and sorghum dw3 mutants. *Science* **302**, 81–84.

955 **O'Connor, D. L., Runions, A., Sluis, A., Bragg, J., Vogel, J. P., Prusinkiewicz,**
956 **P. and Hake, S.** (2014). A division in PIN-mediated auxin patterning during
957 organ initiation in grasses. *PLoS Comput Biol* **10**, e1003447.

958 **Okada, K., Ueda, J., Komaki, M. K., Bell, C. J. and Shimura, Y.** (1991).

959 Requirement of the Auxin Polar Transport System in Early Stages of
960 Arabidopsis Floral Bud Formation. *The Plant Cell* **3**, 677–684.

961 **Paponov, I. A., Teale, W. D. and Trebar, M.** (2005). The PIN auxin efflux
962 facilitators: evolutionary and functional perspectives. *Trends Plant Sci* **10**,
963 170–177.

964 **Prusinkiewicz, P., Crawford, S., Smith, R. S., Ljung, K., Bennett, T. A.,**
965 **Ongaro, V. and Leyser, H. M. O.** (2009). Control of bud activation by an
966 auxin transport switch. *Proc Natl Acad Sci USA* **106**, 17431–17436.

967 **Raven, J. A.** (1975). Transport of indoleacetic acid in plant cells in relation to pH
968 and electrical potential gradients, and its significance for polar IAA transport.
969 *New Phytol* **74**, 163–172.

970 **Reinhardt, D., Mandel, T. and Kuhlemeier, C.** (2000). Auxin Regulates the
971 Initiation and Radial Position of Plant Lateral Organs. *The Plant Cell* **12**, 507.

972 **Reinhardt, D., Pesce, E.-R., Stieger, P., Mandel, T., Baltensperger, K.,**
973 **Bennett, M. J., Traas, J., Friml, J. and Kuhlemeier, C.** (2003). Regulation of
974 phyllotaxis by polar auxin transport. *Nature* **426**, 255–260.

975 **Rubery, P. H. and Sheldrake, A. R.** (1974). Carrier-mediated auxin transport.
976 *Planta* **118**, 101–121.

977 **Sauer, M., Balla, J., Luschnig, C., Wisniewska, J., Reinöhl, V., Friml, J. and**
978 **Benková, E.** (2006). Canalization of auxin flow by Aux/IAA-ARF-dependent
979 feedback regulation of PIN polarity. *Genes Dev* **20**, 2902–2911.

980 **Sawchuk, M. G., Edgar, A. and Scarpella, E.** (2013). Patterning of Leaf Vein
981 Networks by Convergent Auxin Transport Pathways. *PLoS Genet* **9**,
982 e1003294.

983 **Scarpella, E., Marcos, D., Friml, J. and Berleth, T.** (2006). Control of leaf
984 vascular patterning by polar auxin transport. *Genes Dev* **20**, 1015–1027.

985 **Sessions, A., Weigel, D. and Yanofsky, M. F.** (2002). The Arabidopsis thaliana
986 MERISTEM LAYER 1 promoter specifies epidermal expression in meristems
987 and young primordia. *Plant J* **20**, 259–263.

988 **Shinohara, N., Taylor, C. and Leyser, H. M. O.** (2013). Strigolactone Can
989 Promote or Inhibit Shoot Branching by Triggering Rapid Depletion of the
990 Auxin Efflux Protein PIN1 from the Plasma Membrane. *PLoS Biol* **11**,
991 e1001474.

992 **Smith, R. S., Guyomarc'h, S., Mandel, T., Reinhardt, D., Kuhlemeier, C. and**
993 **Prusinkiewicz, P.** (2006). A plausible model of phyllotaxis. *Proc. Natl. Acad.*
994 *Sci. U.S.A.* **103**, 1301–1306.

995 **Stoma, S., Lucas, M., Chopard, J., Schaedel, M. and Godin, C.** (2008). Flux-
996 Based Transport Enhancement as a Plausible Unifying Mechanism for Auxin
997 Transport in Meristem Development. *PLoS Comput Biol* **4**, e1000207.

998 **Torii, K. U., Mitsukawa, N., Oosumi, T., Matsuura, Y., Yokoyama, R., Whittier,**
999 **R. F. and Komeda, Y.** (1996). The Arabidopsis ERECTA gene encodes a
1000 putative receptor protein kinase with extracellular leucine-rich repeats. *The*
1001 *Plant Cell* **8**, 735–746.

1002 **Verna, C., Sawchuk, M. G., Linh, N. M. and Scarpella, E.** (2015). Control of
1003 vein network topology by auxin transport. *BMC Biol* **13**, 94.

1004 **Vieten, A., Vanneste, S., Wisniewska, J., Benkova, E., Benjamins, R.,**
1005 **Beeckman, T., Luschnig, C. and Friml, J.** (2005). Functional redundancy of
1006 PIN proteins is accompanied by auxin-dependent cross-regulation of PIN
1007 expression. *Development* **132**, 4521–4531.

1008 **Wang, R. and Estelle, M.** (2014). Diversity and specificity: auxin perception and
1009 signaling through the TIR1/AFB pathway. *Curr Opin Plant Biol* **21**, 51–58.

1010 **Weller, B., Zourelidou, M., Frank, L., Barbosa, I. C. R., Fastner, A., Richter,**
1011 **S., Jürgens, G., Hammes, U. Z. and Schwechheimer, C.** (2017). Dynamic
1012 PIN-FORMED auxin efflux carrier phosphorylation at the plasma membrane
1013 controls auxin efflux-dependent growth. *Proc Natl Acad Sci USA* **114**, E887–
1014 E896.

1015 **Willige, B. C., Ahlers, S., Zourelidou, M., Barbosa, I. C. R., Demarsy, E.,**
1016 **Trevisan, M., Davis, P. A., Roelfsema, M. R. G., Hangarter, R.,**
1017 **Fankhauser, C., et al.** (2013). D6PK AGCVIII kinases are required for auxin
1018 transport and phototropic hypocotyl bending in Arabidopsis. *The Plant Cell* **25**,
1019 1674–1688.

1020 **Wisniewska, J., Xu, J., Seifertová, D., Brewer, P. B., Ruzicka, K., Blilou, I.,**
1021 **Rouquié, D., Benková, E., Scheres, B. and Friml, J.** (2006). Polar PIN
1022 localization directs auxin flow in plants. *Science* **312**, 883–883.

1023 **Xu, J., Hofhuis, H., Heidstra, R., Sauer, M., Friml, J. and Scheres, B.** (2006).
1024 A molecular framework for plant regeneration. *Science* **311**, 385–388.

1025 **Zhou, C., Han, L., Hou, C., Metelli, A., Qi, L., Tadege, M., Mysore, K. S. and**
1026 **Wang, Z.-Y.** (2011). Developmental analysis of a Medicago truncatula

1027 smooth leaf margin1 mutant reveals context-dependent effects on compound
1028 leaf development. *The Plant Cell* **23**, 2106–2124.

1029

1030

1031 # Figures and Legends

1032 **Figure 1. Mutation of SoPIN1 but not PIN1a and PIN1b severely effects organ**
1033 **initiation in Brachypodium. (A)** *SoPIN1*, *PIN1a*, and *PIN1b* CRISPR-derived mutant
1034 alleles (see methods). Coding sequences are indicated by grey boxes. Arrowheads
1035 indicate CRISPR target sites and are labeled with the type of DNA lesion (C insertion, T
1036 insertion, or A deletion). All mutant alleles have frame shifts that result in premature
1037 stop codons at the positions indicated. **(B-G)** Inflorescence phenotypes of CRISPR-
1038 derived *sopin1-1, pin1a-1*, and *pin1b-1* mutants. See Figure 2 for whole-plant
1039 phenotypes. **(B-E)** and **(G)** are scanning electron microscopy (SEM). **(B)** Immature wild-
1040 type (WT) (inbred line Bd21-3) Brachypodium inflorescence with several lateral spikelet
1041 meristems (lsm), and a terminal spikelet meristem (tsm). **(C)** *sopin1-1* plants have
1042 severe organ initiation defects in the inflorescence. **(D)** Detail of a wild-type lateral
1043 spikelet meristem outlined by a box in **(B)** showing an immature lemma (l), which is the
1044 leaf-like organ that subtends the floral meristem (fm). **(E)** Detail of barren lateral spikelet
1045 meristem outlined by box in **(C). (F)** Mature inflorescence phenotypes of WT (Inbred
1046 Bd21-3), *sopin1-1, pin1a-1, pin1b-1,* and double *pin1a-1 / pin1b-1* mutants. The terminal
1047 spikelet (ts) of each inflorescence is indicated for comparison. Arrowhead indicates bent
1048 internode tissue in *pin1b-1.* Genotypes for **(G-I)** are indicated at the bottom of **(I). (G)**
1049 SEM details of representative spikelet meristems**. (H)** Box-plot of total whole-plant
1050 spikelet number at seed-set. (n = 22-53 plants each genotype). Samples with different
1051 letters are significantly different from each other (ANOVA, Tukey HSD, $p < 0.05$). See
1052 "Figure 1 H-I Source Data 1" for source data. **(I)** Box-plot of the number of florets in
1053 each terminal spikelet of the central branch at seed set. (n = 22-53 plants each

1054 genotype). Samples with different letters are significantly different from each other
1055 (ANOVA, Tukey HSD, $p < 0.05$). See “Figure 1 H-I Source Data 1” for source data. **(J)**
1056 Medial confocal Z-section of pZmUbi::DII-Venus (DII) expression in a WT spikelet co-
1057 expressing SoPIN1 tagged with Cerulean (a CFP variant) under the native *SoPIN1*
1058 promoter. Organ primordia are numbered I2, I1, P1 from youngest to oldest. DII is
1059 normally degraded at SoPIN1 convergence points in I2 and I1 primordia (asterisks), and
1060 in response to auxin treatment (See Figure 1 – supplement 2). Inset shows color look-
1061 up-table for all subsequent PIN images and color look-up-table for DII. **(K)** Medial
1062 confocal Z-section of pZmUbi::DII-Venus expression in a *sopin1-1* spikelet meristem.
1063 DII degradation does not occur in the periphery of *sopin1-1* meristems, and organs fail
1064 to initiate (arrow). Scale bars: 100μm in **(B)** and **(C)**, 20μm in **(D)** and **(E),** 1cm in **(F),**
1065 50μm each in **(G),** and 25μm in **(J)** and **(K).**
1066
1067 **Figure 1 – supplement 1. *sopin1-1* is complemented by the SoPIN1-CIT reporter.**
1068 **(A)** Wild-type inflorescence (Bd21-3 background) with wild-type mature spikelets (s). **(B)**
1069 *sopin1-1* inflorescence with an aborted spikelet (asterisk) and several barren white
1070 spikelet nodes (n). Green internode (i) tissue is also labeled. **(C)** Inflorescence of a
1071 *sopin1-1* mutant plant complemented by previously published full-length SoPIN1
1072 internal CITRINE fluorescent protein fusion under the native *SoPIN1* promoter
1073 (+SoPIN1-CIT) (O'Connor et al., 2014). (N=34: 6 *sopin1-1* phenotype, 28 wt phenotype)
1074 Scale bars: 1cm.
1075

1076 **Figure 1 – supplement 2. DII-Venus is degraded in the presence of auxin in**
1077 **Brachypodium spikelet meristems. (A)** 1 μM NAA-treated, and **(B)** mock-treated
1078 spikelet meristems expressing pZmUbi::DII-Venus imaged every 30 min after treatment.
1079 Images from left to right, pre-treatment expression, 30 min, 60 min and 90 min time-
1080 points. **(C)** Relative mean fluorescence in a radius at the spikelet meristem tip in NAA-
1081 treated and Mock samples at 0, 30, 60 and 90-minute time points. Scale bars: 25μm.
1082
1083 **Figure 1 - Source Data 1.** Source data for spikelet and floret counts in Figure 1 H-I.
1084
1085 **Figure 1 – Source Data 2.** Source data for DII quantification in Figure 1 – supplement 2
1086 panel C.
1087
1088

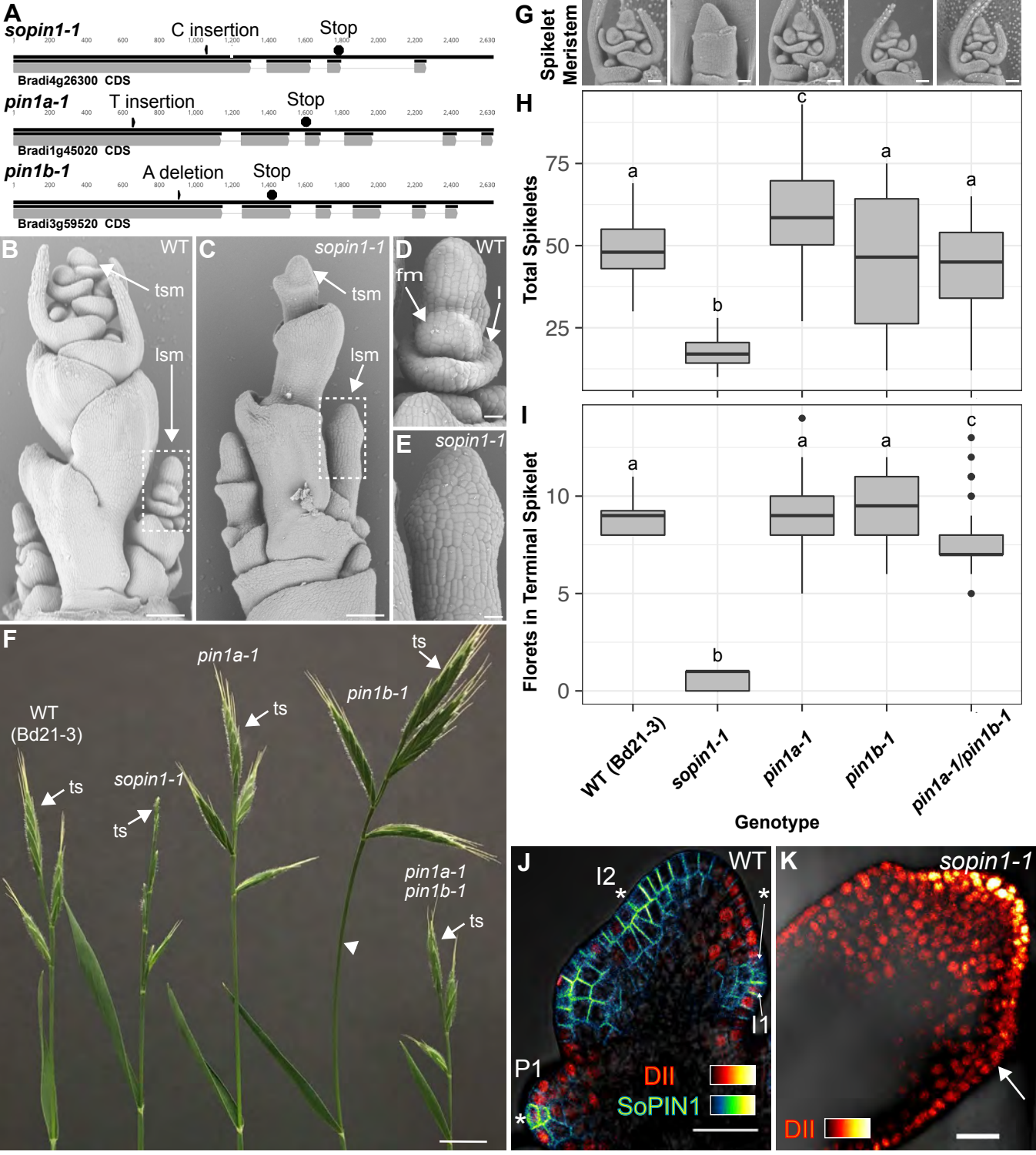
A
sopin1-1
C insertion
Stop
Bradi4g26300 CDS
pin1a-1
T insertion
Stop
Bradi1g45020 CDS
pin1b-1
A deletion
Stop
Bradi3g59520 CDS
B
WT
tsm
lsm
C
sopin1-1
tsm
lsm
D
WT
fm
l
E
sopin1-1
F
WT
(Bd21-3)
ts
sopin1-1
ts
pin1a-1
ts
pin1b-1
ts
pin1a-1
pin1b-1
ts
G
Spikelet
Meristem
H
Total Spikelets
75
50
25
a
b
c
a
a
I
Florets in Terminal Spikelet
10
5
0
a
b
a
a
c
WT (Bd21-3)
sopin1-1
pin1a-1
pin1b-1
pin1a-1/pin1b-1
Genotype
J
WT
I2
I1
P1
DII
SoPIN1
K
sopin1-1
DII

Figure 1

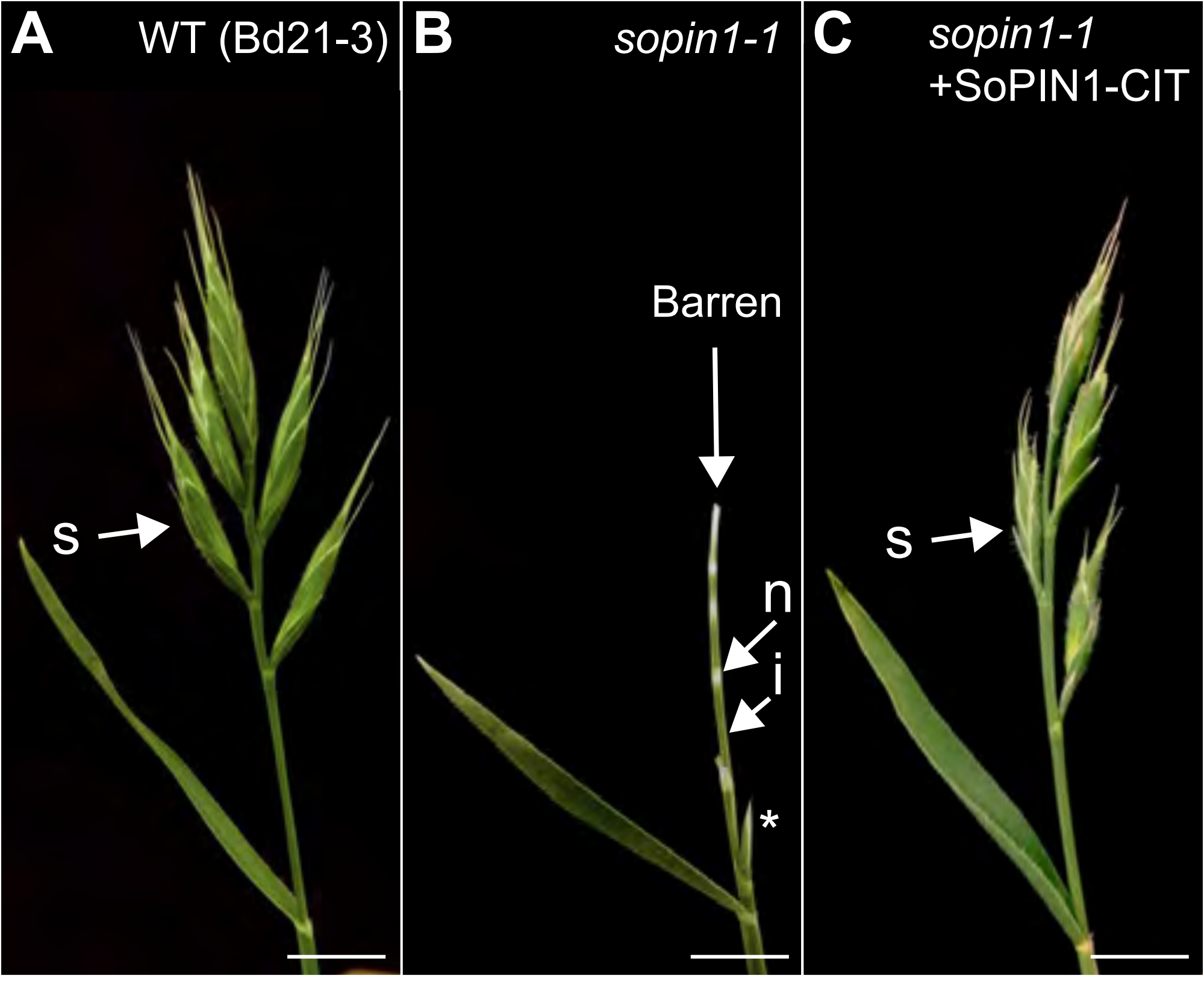

Figure 1 - supplement 1

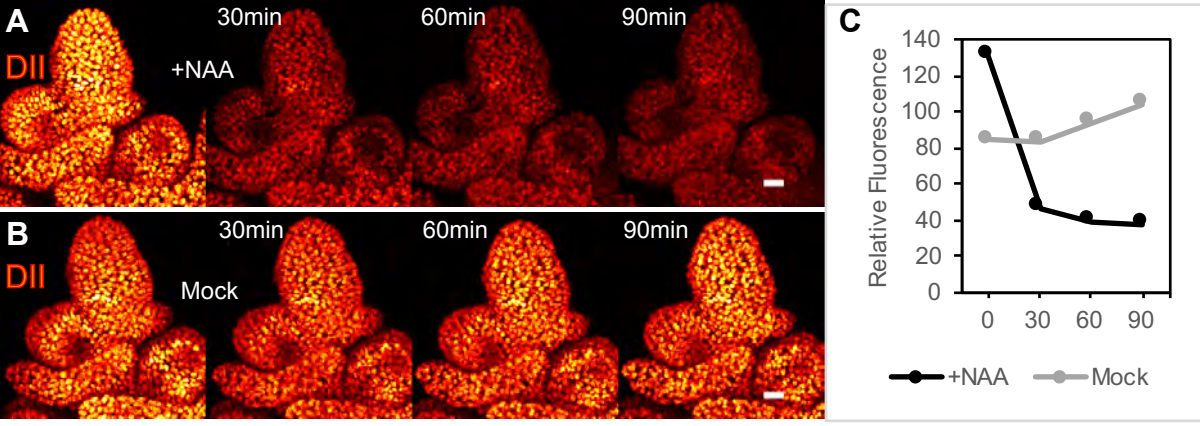

Figure 1 - supplement 2

1089 **Figure 2 - PIN1a and PIN1b redundantly control internode growth in**
1090 **Brachypodium. (A-D)** Whole-plant phenotypes for WT (Bd21-3), *pin1a-1*, *pin1b-1*, and
1091 double *pin1a-1 / pin1b-1* mutants. **(E)** Stacked bar graph of the length of the first 5
1092 internodes below the inflorescence of the main branch, labeled I1-I5 from top to bottom.
1093 Lines connect analogous internodes between genotypes. Analogous internodes with
1094 different letters are significantly different from each other (ANOVA, Tukey HSD, $p <$
1095 0.05). I5 internodes were not significantly different between genotypes and are
1096 unlabeled. Internode lengths significantly different from WT are indicated by asterisks.
1097 (n = 18-51 individuals each genotype) See "Figure 2 Source Data 1" for source data.
1098 Scale bars: 1cm in **(A-D)**.
1099
1100 **Figure 2 – supplement 1. PIN1b-CIT-mediated complementation of *pin1b-1***
1101 **internode length defects.** Stacked bar graph of the length of the first 5 internodes
1102 below the inflorescence of the main branch, labeled I1-I5 from top to bottom, for *pin1b-1*
1103 and *pin1b-1* containing the previously published full-length PIN1b internal CITRINE
1104 fluorescent protein fusion under the native *PIN1b* promoter (+PIN1b-CIT) (O'Connor et
1105 al., 2014) (n = 10 each genotype). Lines connect analogous internodes between
1106 genotypes. Internodes that are significantly different between genotypes are marked
1107 with asterisks. The I4 and I5 internodes are significantly shorter in the complemented
1108 line than in *pin1b-1* (ANOVA, Tukey HSD, $p < 0.05$). See "Figure 2 Source Data 2" for
1109 source data.
1110
1111 **Figure 2 - Source Data 1.** Source data for internode length measurements in Figure 2E.

1112

1113 **Figure 2 - Source Data 2.** Source data for PIN1b-CIT-mediated complementation of

1114 *pin1b-1* internode lengths in Figure 2 - supplement 1.

1115

1116

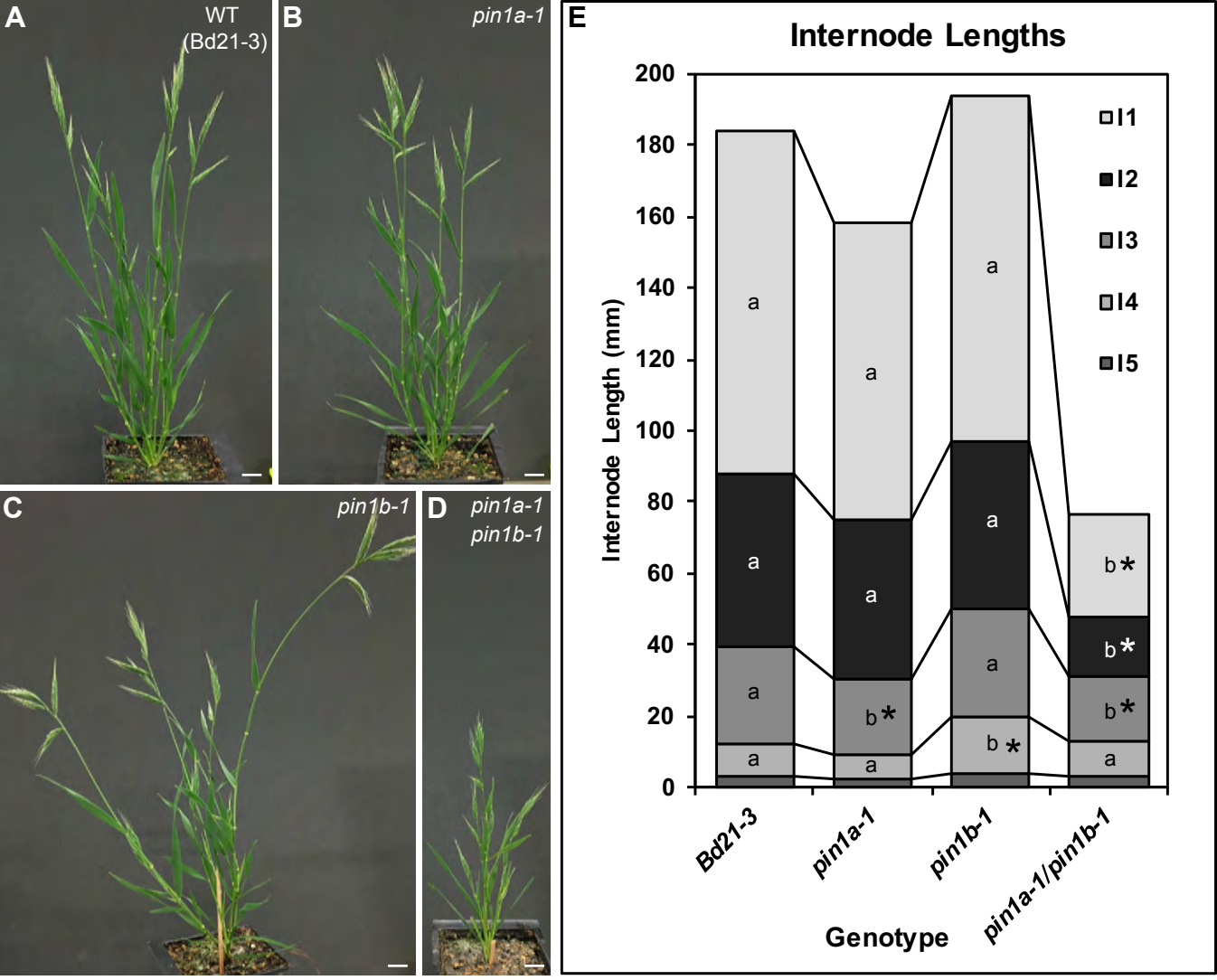
A
WT
(Bd21-3)
B
pin1a-1
C
pin1b-1
D
pin1a-1
pin1b-1
E
Internode Lengths
Internode Length (mm)
0
20
40
60
80
100
120
140
160
180
200
I1
I2
I3
I4
I5
a
b*
Bd21-3
pin1a-1
pin1b-1
pin1a-1/pin1b-1
Genotype

Figure 2

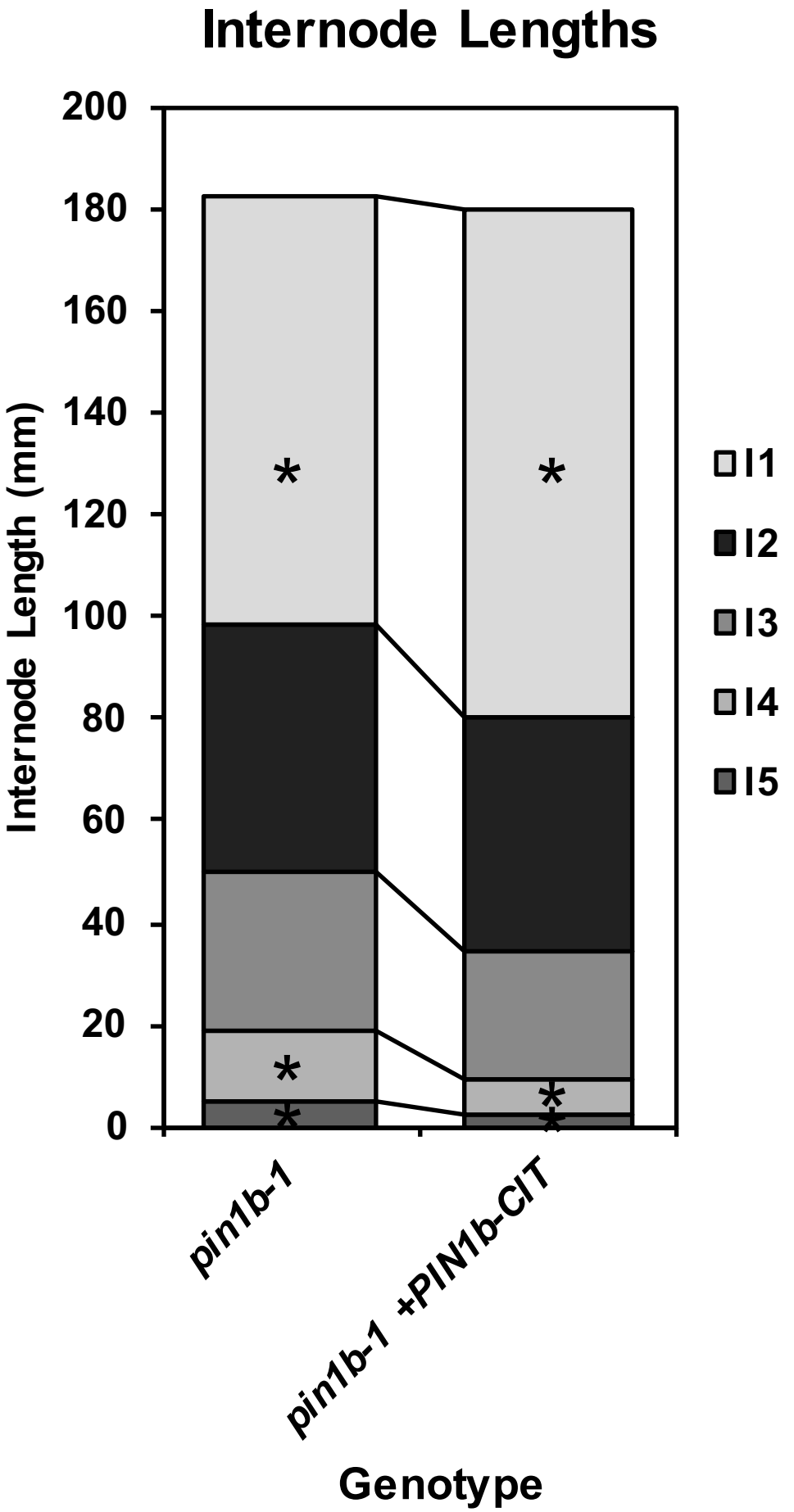

Figure 2 - supplement 1

1117 **Figure 3. AtPIN1, SoPIN1, and PIN1b show different behaviors when expressed in**
1118 **wild-type Arabidopsis.** Arabidopsis *AtPIN1* promoter (*proAtPIN1*) driven expression of
1119 GFP-tagged AtPIN1 and CITRINE-tagged (a YFP derivative) SoPIN1 and PIN1b in wild-
1120 type Columbia (Col-0) Arabidopsis. **(A,D,G,J)** AtPIN1, **(B,E,H,K)** SoPIN1, **(C,F,I,L)**
1121 PIN1b. **(A-C)** Maximum projections of meristem apexes. Arrows in (**A)** and **(B)** indicate
1122 convergence points (cp) in I2 primordium. Arrowhead in **(C)** indicates internalized PIN1b
1123 in punctate membrane bodies. The I2 and I1 primordia are labeled. **(D-F)** Tiled confocal
1124 maximum projections of longitudinal hand-sections through inflorescence apexes.
1125 Arrows indicate SoPIN1 epidermal expression in sepal primordia and flower pedicels in
1126 **(E)** and the lack of AtPIN1 and PIN1b epidermal expression in the same tissues in **(D)**
1127 and **(F)**. Box in **(D)** shows detail area in Figure 3 – supplement 1 panel D**. (G-I)** Tiled
1128 confocal maximum projections of longitudinal hand-sections through basal inflorescence
1129 stem internodes 1cm above the rosette. **(J-L)** Tiled confocal maximum projections of
1130 hand cross-sections through basal internodes 1cm above the rosette. Signal at the edge
1131 of each section (arrowheads) is cuticle auto-florescence. The cortex (co), cambium (ca),
1132 xylem parenchyma (xp), and pith (p) tissues are indicated in **(G-L)**. Arrows in **(H)** and
1133 **(K)** indicate cortex and pith ectopic expression of SoPIN1. Red signal in all panels is
1134 chlorophyll auto-florescence. Scale bars: 25μm in **(A-C)**, and 100μm in **(D-L)**.
1135
1136 **Figure 3 – supplement 1. *proAtPIN1* AtPIN1, SoPIN1, and PIN1b expression details.**
1137 **(A)** Confocal z-section of AtPIN1 accumulation in vascular-associated domains just
1138 below the apex of the meristem shown in Figure 3A. **(B)** Confocal z-section of SoPIN1
1139 accumulation in a ring-shaped domain just below the apex of the meristem shown in

1140 Figure 3B. **(C)** Confocal z-section of PIN1b accumulation in vascular-associated
1141 domains just below the apex of the meristem shown in Figure 3C. (**D)** Maximum
1142 projection detail of AtPIN1 accumulation in both pith (p) and procambium (pc) tissues in
1143 the immature inflorescence stem outlined with a box in Figure 3D. **(E)** Maximum
1144 projection detail of rootward polarized SoPIN1 (arrows) in a longitudinal hand-section of
1145 the basal internode pith tissue. **(F)** Maximum projection detail of rootward polarized
1146 PIN1b (arrows) in a longitudinal hand-section of the basal internode xylem parenchyma
1147 tissue. Red signal in **(D-F)** is chlorophyll auto-florescence. Scale bars: 25μm.
1148
1149

Wildtype (Col-0)

proAtPIN1::AtPIN1 | *proAtPIN1*::SoPIN1 | *proAtPIN1*::PIN1b

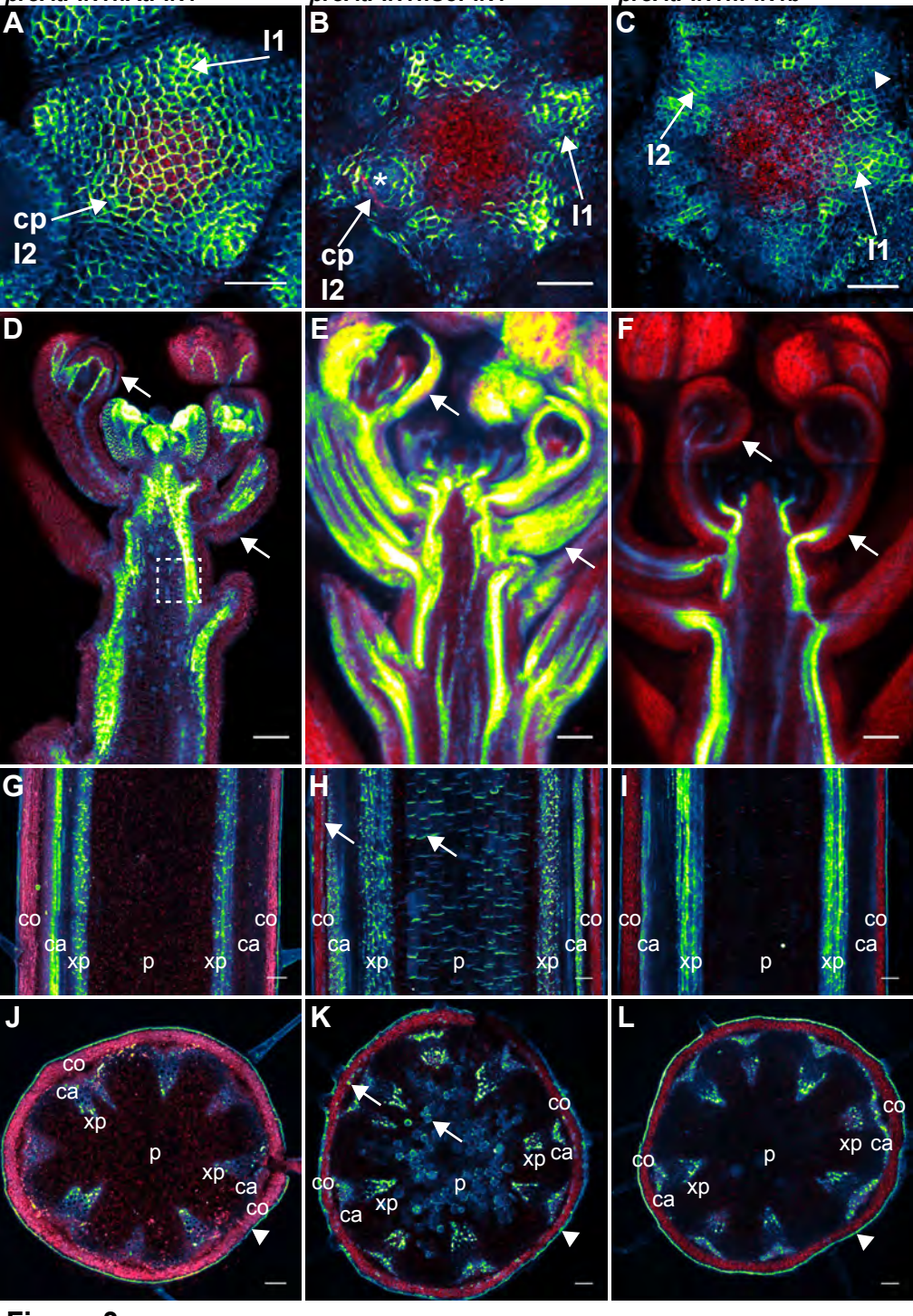

Figure 3

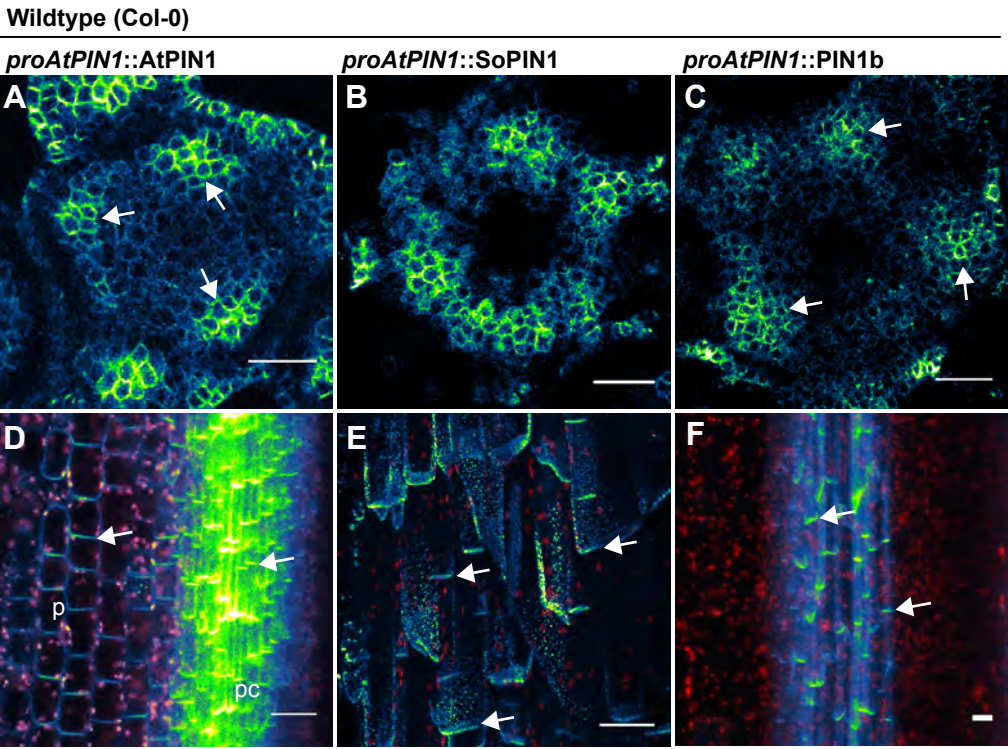

Figure 3 - supplement 1

1150 **Figure 4. SoPIN1 but not PIN1b can partially complement the Arabidopsis *pin1-***
1151 ***613* mutant organ initiation and bulk transport defects. (A)** From left to right,
1152 inflorescence phenotypes of WT (Col-0), *proAtPIN1::*SoPIN1 in *pin1-613,*
1153 *proAtPIN1*::PIN1b in *pin1-613,* and *pin1-613* alone. Note that PIN1b-expressing *pin1-*
1154 *613* plants are indistinguishable from *pin1-613* alone. See Figure 4 - supplement 1 for
1155 whole-plant phenotypes. **(B)** Flower (left), and inflorescence apex (right) of WT (Col-0).
1156 **(C)** Flower (left), and inflorescence apex (right) of *proAtPIN1::*SoPIN1 complemented
1157 *pin1-613* mutants. Note the increase in petal number and lack of stamens in the flower,
1158 see Figure 4 - supplement 2 for organ counts. **(D)** Box-plot of bulk auxin transport
1159 (counts per minute, CPM) through basal internodes 1cm above the rosette of 40-day-old
1160 Arabidopsis inflorescence stems. (n=16 each genotype). Samples with different letters
1161 are significantly different from each other (ANOVA, Tukey HSD, $p < 0.05$). See Figure 3
1162 - Source Data 1 for source data. Scale bars: 1cm in **(A)**, 1mm in **(B-C)**.
1163
1164 **Figure 4 - supplement 1. Whole-plant phenotypes of *proAtPIN1*-driven**
1165 **complementation of *pin1-613.*** From left to right, Col-0 (WT), *proAtPIN1::*SoPIN1
1166 complemented *pin1-613*, *proAtPIN1::*PIN1b expressing *pin1-613,* and *pin1-613* alone.
1167 Scale bar: 1cm.
1168
1169 **Figure 4 - supplement 2. Floral organ number in *proAtPIN1::*SoPIN1**
1170 **complemented flowers.** Mean and standard-error of sepal, petal, stamen and carpel
1171 organ numbers in heterozygous *pin1-613* or wild-type (white bars), and

1172 *proAtPIN1::*SoPIN1-complemented *pin1-613* flowers (grey bars) (n=30). See Figure 4 -
1173 Source Data 2 for source data.
1174
1175 **Figure 4 - Source Data 1. Source data for Figure 4D auxin transport assays.**
1176
1177 **Figure 4 - Source Data 2. Source data for Figure 4 - supplement 2 floral organ**
1178 **numbers.**
1179
1180

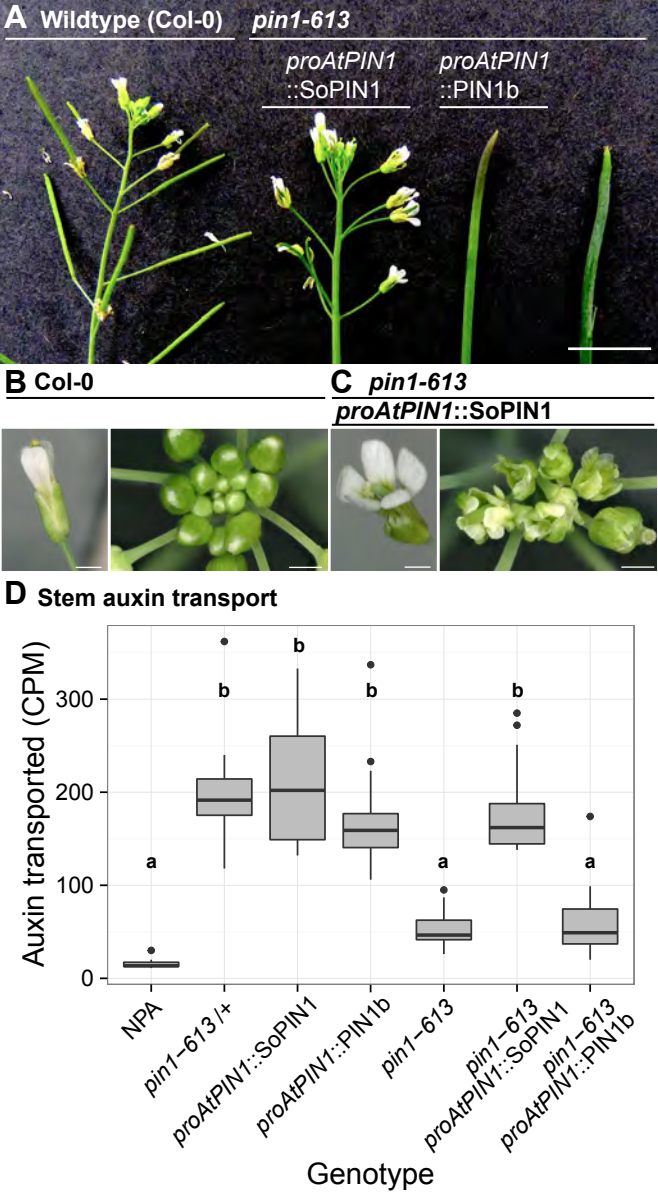
A
Wildtype (Col-0)
pin1-613
proAtPIN1 ::SoPIN1
proAtPIN1 ::PIN1b
B
Col-0
C
pin1-613
proAtPIN1::SoPIN1
D
Stem auxin transport
Auxin transported (CPM)
0
100
200
300
a
b
b
b
a
b
a
NPA
pin1−613/+
proAtPIN1::SoPIN1
proAtPIN1::PIN1b
pin1−613
pin1−613 proAtPIN1::SoPIN1
pin1−613 proAtPIN1::PIN1b
Genotype

Figure 4

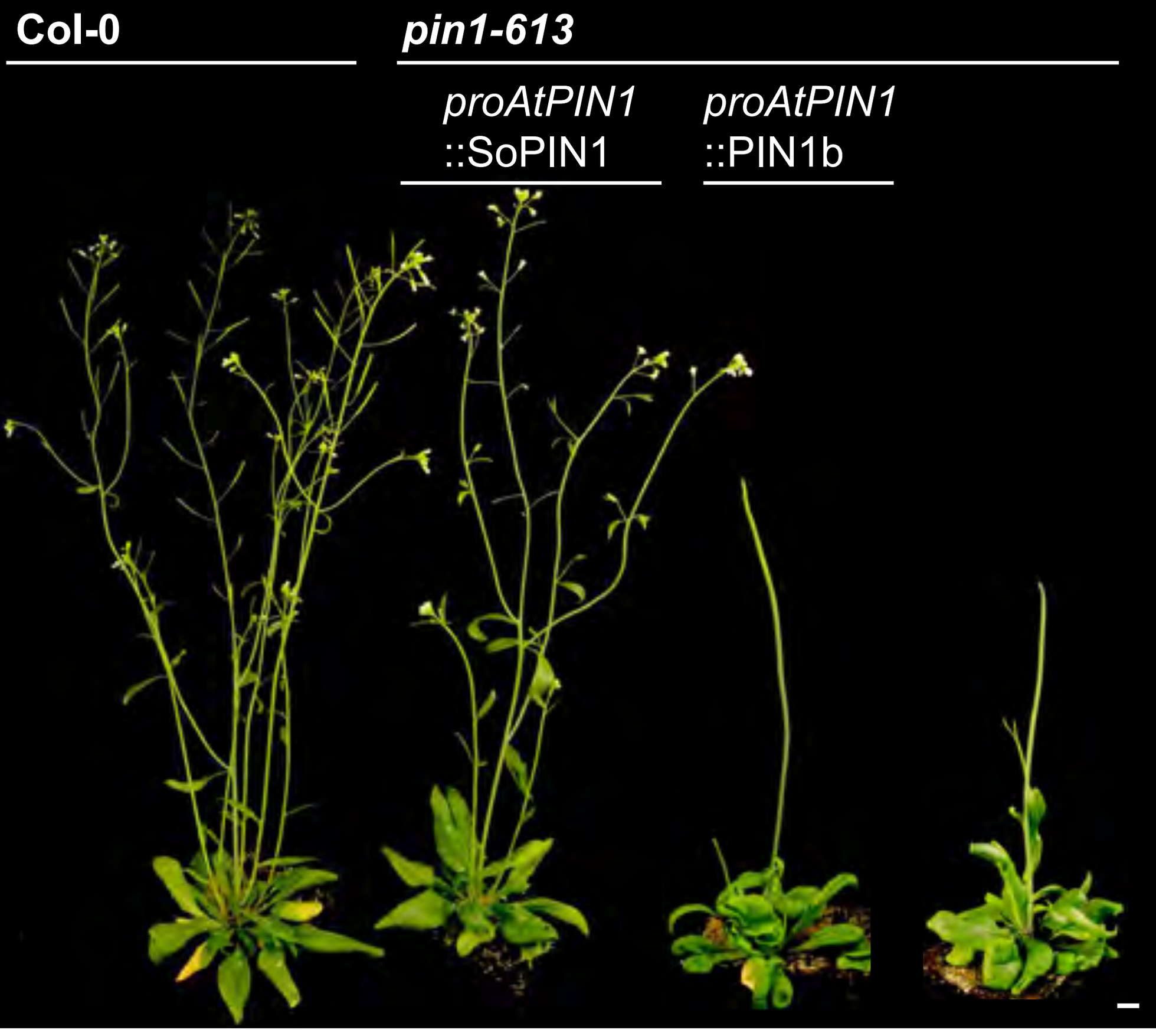

Figure 4 - supplement 1

Floral organ number - *proAtPIN1::*SoPIN1

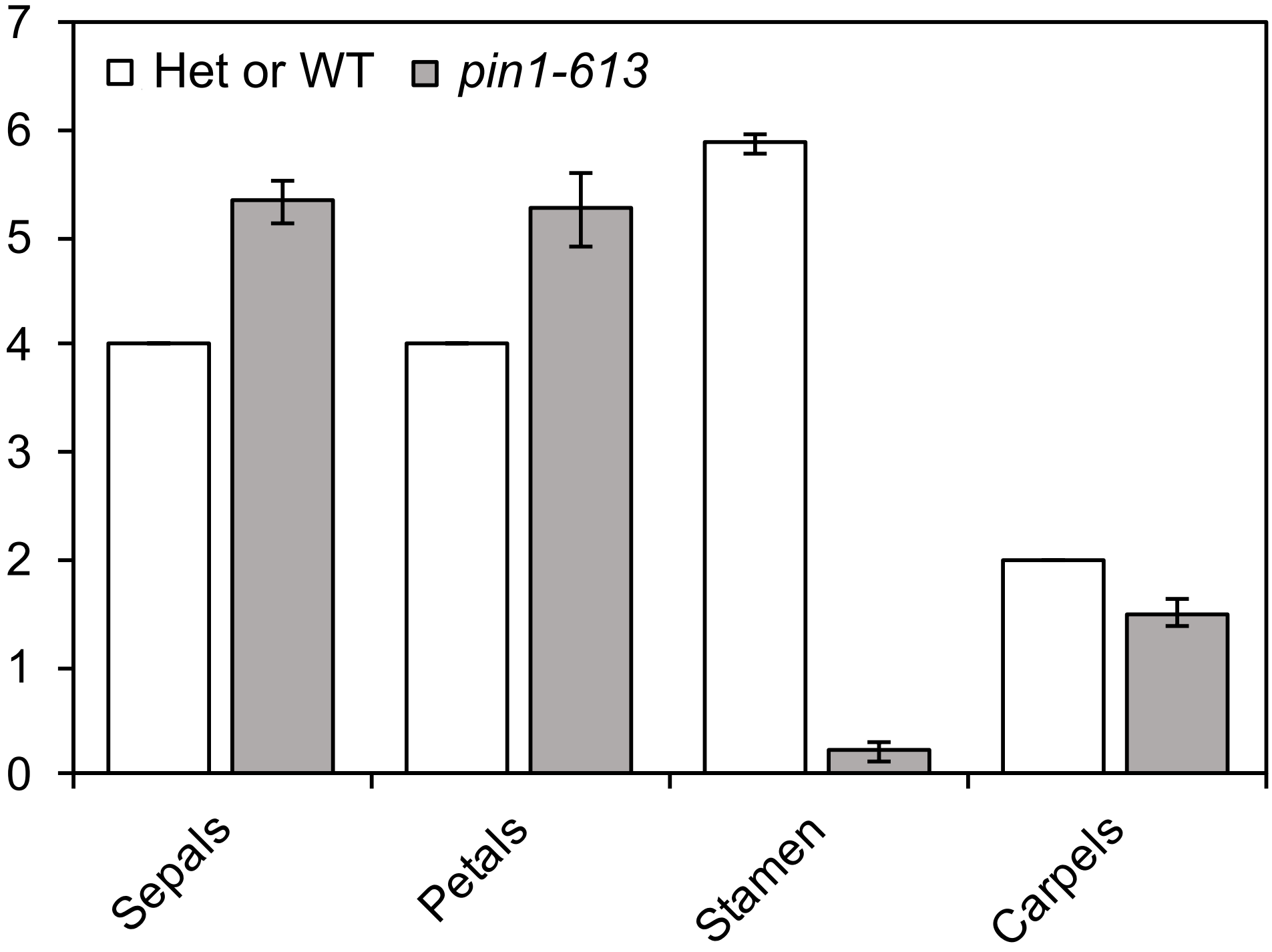

Figure 4 - supplement 2

1181 **Figure 5. SoPIN1 and PIN1b localization in null *pin1-613* mutants.** Arabidopsis *PIN1*
1182 promoter (*proAtPIN1*) driven expression of Citrine-tagged (YFP derivative) SoPIN1 and
1183 PIN1b in null *pin1-613* mutant tissue. **(A,C,E,G,I)** SoPIN1, **(B,D,F,H,J,K,L,M)** PIN1b. **(A-**
1184 **B)** Maximum projections of meristem apexes. Arrow in **(B)** indicates PIN1b ring shaped
1185 epidermal domain. See Figure 5 – supplement 1 for SoPIN1 expression in a *pin1-613*
1186 segregating family. See Figure 5 – supplement 2 for more examples of PIN1b
1187 expression in *pin1-613* apexes. **(C-D)** Tiled confocal maximum projections of
1188 longitudinal hand-sections through apexes. Arrow in **(D)** indicates increased PIN1b in
1189 the epidermis in the *pin1-613* background. **(E-F)** Tiled maximum projections of
1190 longitudinal hand-sections through basal inflorescence stem internodes 1cm above the
1191 rosette. **(G-H)** Tiled maximum projections of hand cross-sections through basal
1192 internodes 1cm above the rosette. Signal at the edge of each section (arrowheads) is
1193 cuticle auto-florescence. The cortex (co), cambium (ca), xylem parenchyma (xp), and
1194 pith (p) tissues are indicated in **(E-H).** Arrows in **(E)** and **(G)** indicate cortex and pith
1195 accumulation of SoPIN1. **(I)** Confocal z-section of SoPIN1 accumulation in a ring-
1196 shaped domain just below the apex of a complemented *pin1-613* meristem. **(J)**
1197 Longitudinal hand-section of PIN1b just below a *pin1-613* meristem apex. Arrow shows
1198 rootward polarized PIN1b. **(K)** Detail of polarized PIN1b in the meristem epidermis of a
1199 *pin1-613* meristem apex. **(L)** Cross-section of PIN1b (arrow) in distinct bundles 2mm
1200 below a *pin1-613* meristem apex. **(M)** Rootward polarization of PIN1b (arrow) 3-4 mm
1201 below the apex of a *pin1-613* meristem. Red signal in all panels is chlorophyll auto-
1202 florescence. Scale bars: 25μm in **(A-B),** 100μm in **(C-H),** and 25μm in **(I-M)**.
1203

1204 **Figure 5 – supplement 1. *proAtPIN1::*SoPIN1 expression in *pin1-613* segregating**
1205 **family. (A)** *proAtPIN1::*SoPIN1 expression in 6 different WT or heterozygous *pin1-613*
1206 meristem samples. **(B)** *proAtPIN1::*SoPIN1 expression in 6 different complemented
1207 *pin1-613* meristems. All samples were imaged with identical settings to show the
1208 increase in SoPIN1 accumulation in the *pin1-613* mutant background. Red signal is
1209 chlorophyll auto-florescence. Scale bars: 25µm.
1210
1211 **Figure 5 – supplement 2. *proAtPIN1::*PIN1b expression in *pin1-613* apexes.** Two
1212 representative meristems each from four different transgenic events. All samples were
1213 imaged with identical settings. Scale bars: 25µm.
1214
1215

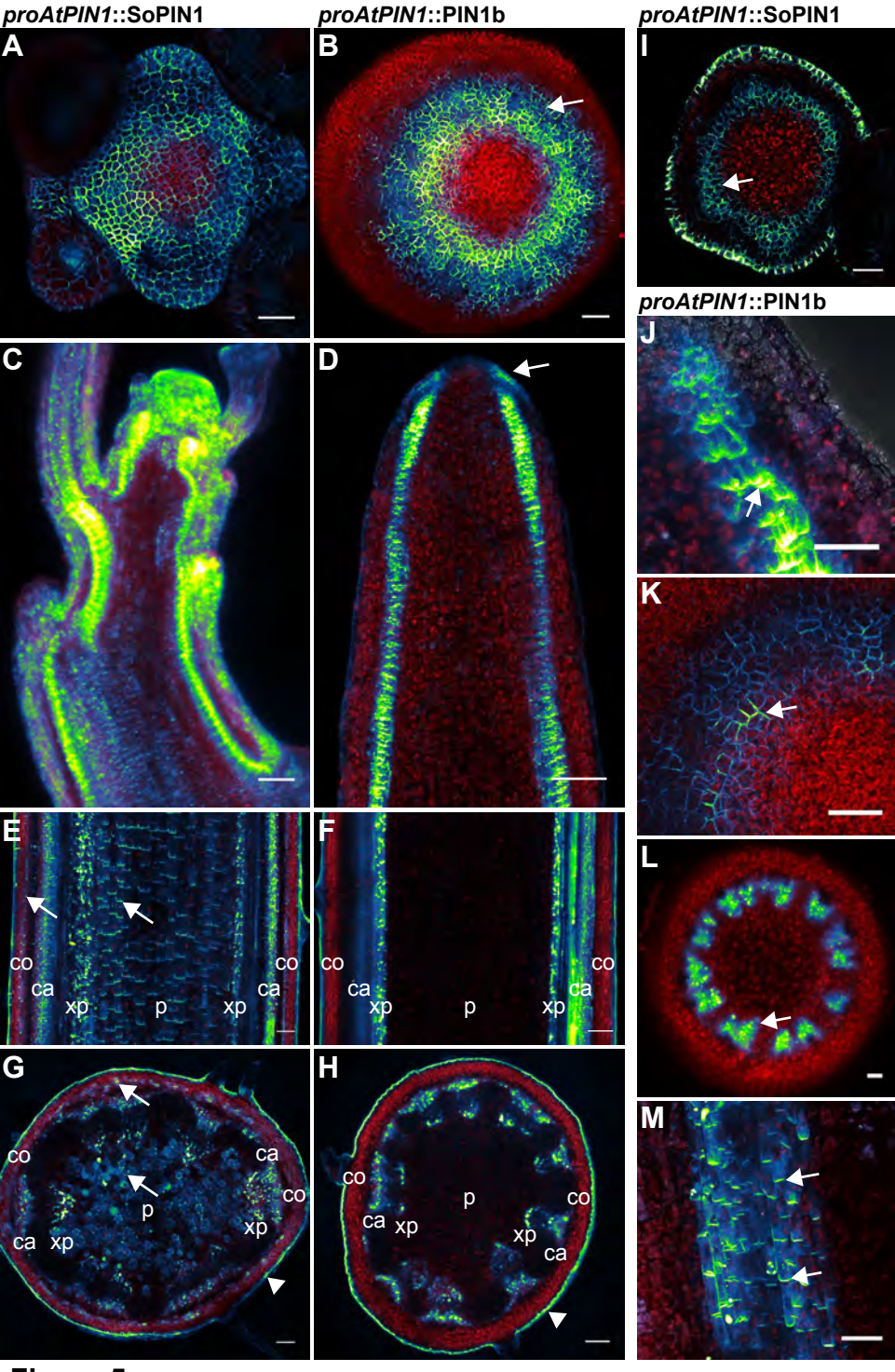
proAtPIN1::SoPIN1
proAtPIN1::PIN1b
proAtPIN1::SoPIN1
proAtPIN1::PIN1b
A
B
I
C
D
J
K
E
F
L
G
H
M
co
ca
xp
p

Figure 5

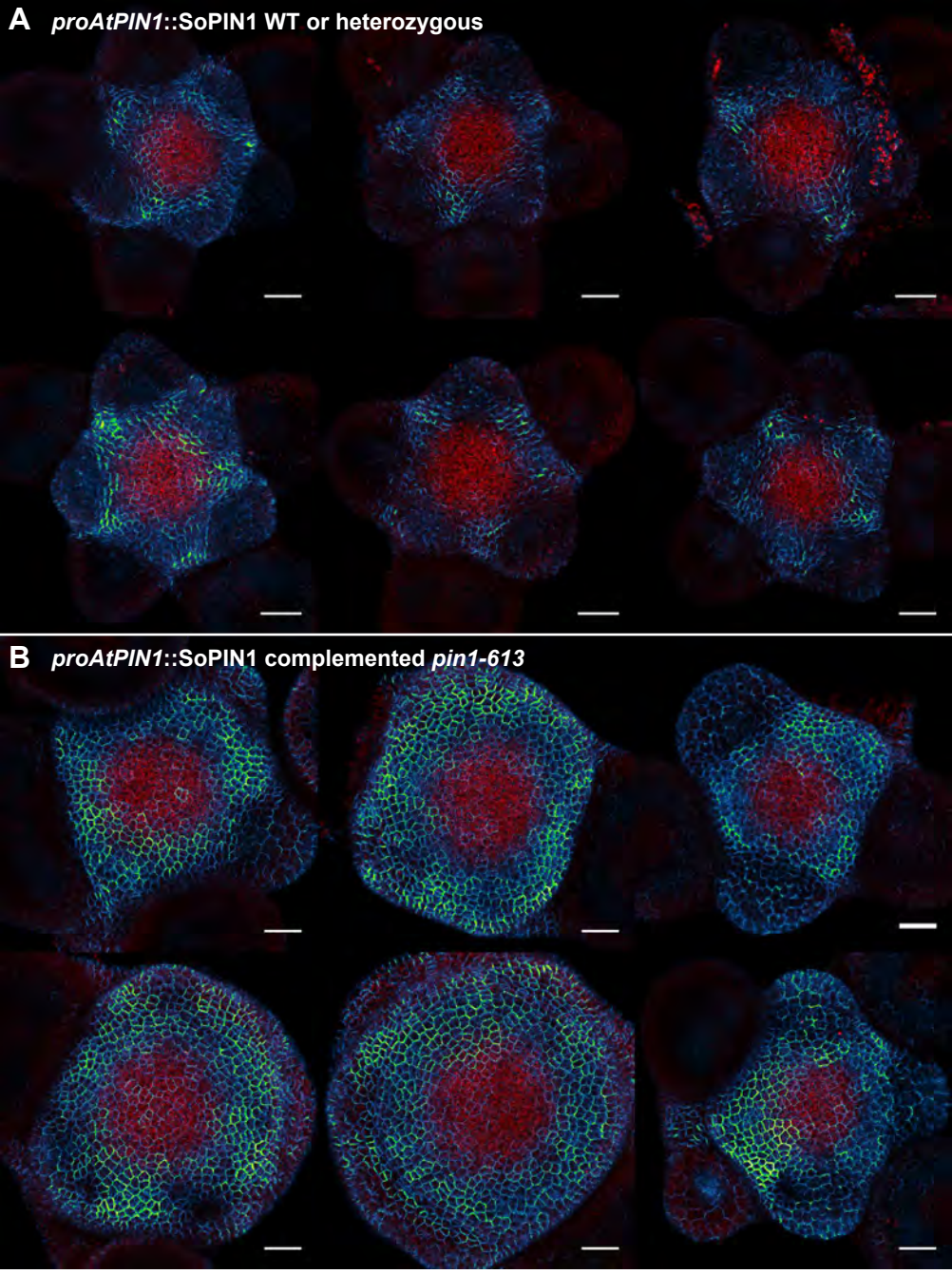

Figure 5 - supplement 1

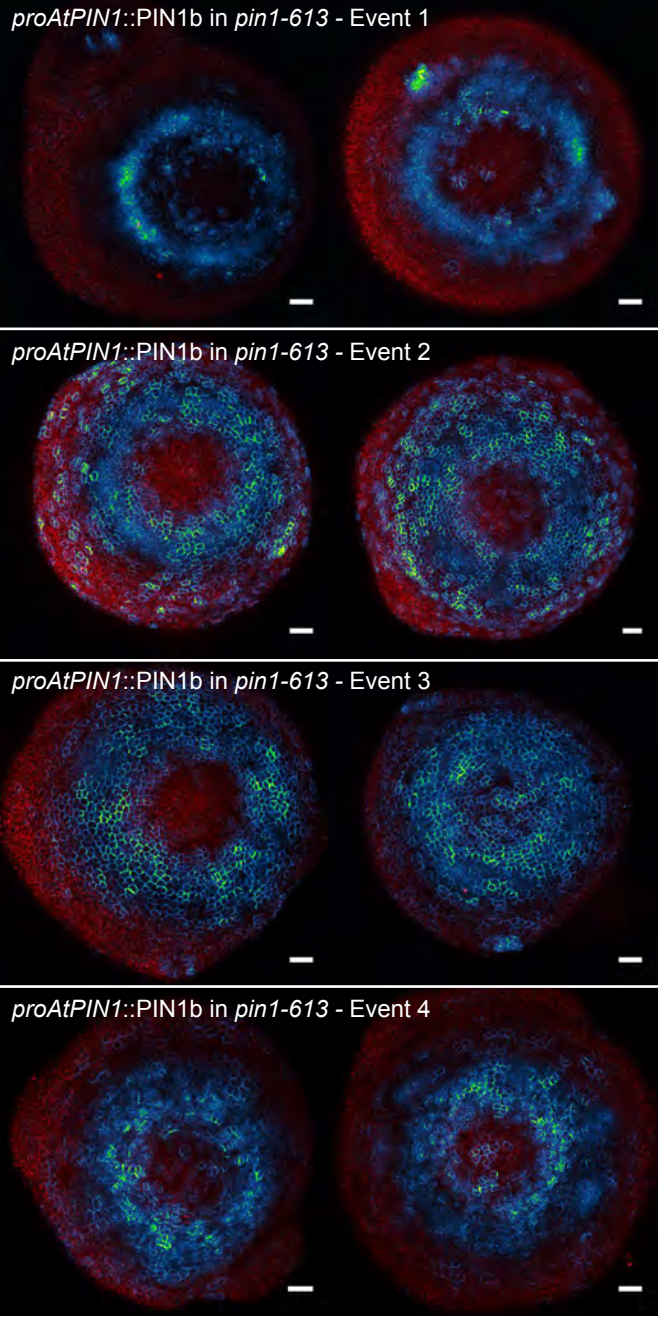

Figure 5 - supplement 2

1216 **Figure 6. SoPIN1 and PIN1b show different behaviors under *proAtML1*-driven**
1217 **expression.** Maximum projections of *proAtML1::*LhG4 driving pOP::SoPIN1 or
1218 pOP::PIN1b (*proAtML1*>>SoPIN1 and *proAtML1*>>PIN1b) in wild-type Landsberg
1219 *erecta* (L*er)* **(A-D),** and *pin1-4* **(E-L)** inflorescence meristems and basal internodes. **(A)**
1220 SoPIN1 and **(B)** PIN1b maximum projections of wild-type L*er* inflorescence meristems.
1221 I3, I2, I1, and P1 primordia are indicated. White boxes around each I2 primordium
1222 indicate the regions detailed in **(C-D).** Asterisk in **(C)** indicates convergence point. Arrow
1223 in **(D)** indicates punctate PIN1b. **(E)** SoPIN1 and **(F)** PIN1b maximum projections of
1224 complemented *pin1-4* meristems. I3, I2, I1, and P1 primordia are indicated. White boxes
1225 around each I2 primordia indicate the regions detailed in **(G-H)**. Asterisks mark
1226 convergence points in **(G)** and **(H)**. Red signal in **(C,D,G,H)** is cell wall propidium iodide
1227 staining. See Figure 6 – supplement 1 for additional samples of *proAtML1*>>SoPIN1
1228 and Figure 6 – supplement 2 for additional samples of *proAtML1*>>PIN1b in both WT
1229 and *pin1-4* meristems*.* See Figure 6 - supplement 3 for details of PIN1b epidermal
1230 intracellular localization in WT and *pin1-4* meristem apexes*.* **(I-J)** Tiled maximum
1231 projections of cross hand-sections of the basal internode of SoPIN1 **(I)** and PIN1b **(J)** -
1232 complemented *pin1-4* plants showing PIN signal in the outer cortex layers (arrows). Red
1233 signal in **(I-J)** is chlorophyll auto-florescence. **(K-L)** Epidermal maximum projections
1234 showing rootward polarized PIN localization (arrows) in the basal internode of SoPIN1
1235 **(K),** and PIN1b **(L)** -complemented *pin1-4* plants. Scale bars: 25μm in **(A-H)**. 100μm in
1236 **(I-L)**.
1237

1238 **Figure 6 – supplement 1. *proAtML1*>>SoPIN1 representative meristem maximum**
1239 **projections. (A)** *proAtML1*>>SoPIN1 expression in three different wild-type L*er*
1240 meristems. **(B)** *proAtML1*>>SoPIN1 expression in three different complemented *pin1-4*
1241 meristems. Capture settings are identical in all samples. Scale bars: 25µm.
1242
1243 **Figure 6 – supplement 2. *proAtML1*>>PIN1b representative meristem maximum**
1244 **projections. (A)** *proAtML1*>>PIN1b expression in three different wild-type L*er*
1245 meristems. **(B)** *proAtML1*>>PIN1b expression in three different complemented *pin1-4*
1246 meristems. Capture settings are identical in all samples. Scale bars: 25µm.
1247
1248 **Figure 6 – supplement 3. Subcellular localization of PIN1b in wild-type (L*er*) and**
1249 ***pin1-4* meristems. (A)** Wild-type (L*er*) meristem expressing *proAtML1*>>PIN1b. Boxes
1250 numbered 1-3 indicate the positions of detail images in **(B-D). (B)** Organ boundary. **(C)**
1251 Incipient organ. **(D)** Meristem apex. **(E)** *pin1-4* meristem complemented by
1252 *proAtML1*>>PIN1b. Boxes numbered 1-3 indicate the positions of detail images in (**F-H).**
1253 **(F)** Meristem apex. **(G)** Organ boundary. **(H)** Convergence point, indicated by asterisk.
1254 Red signal is FM4-64 vital stain. Scale bars: 5µm.
1255
1256

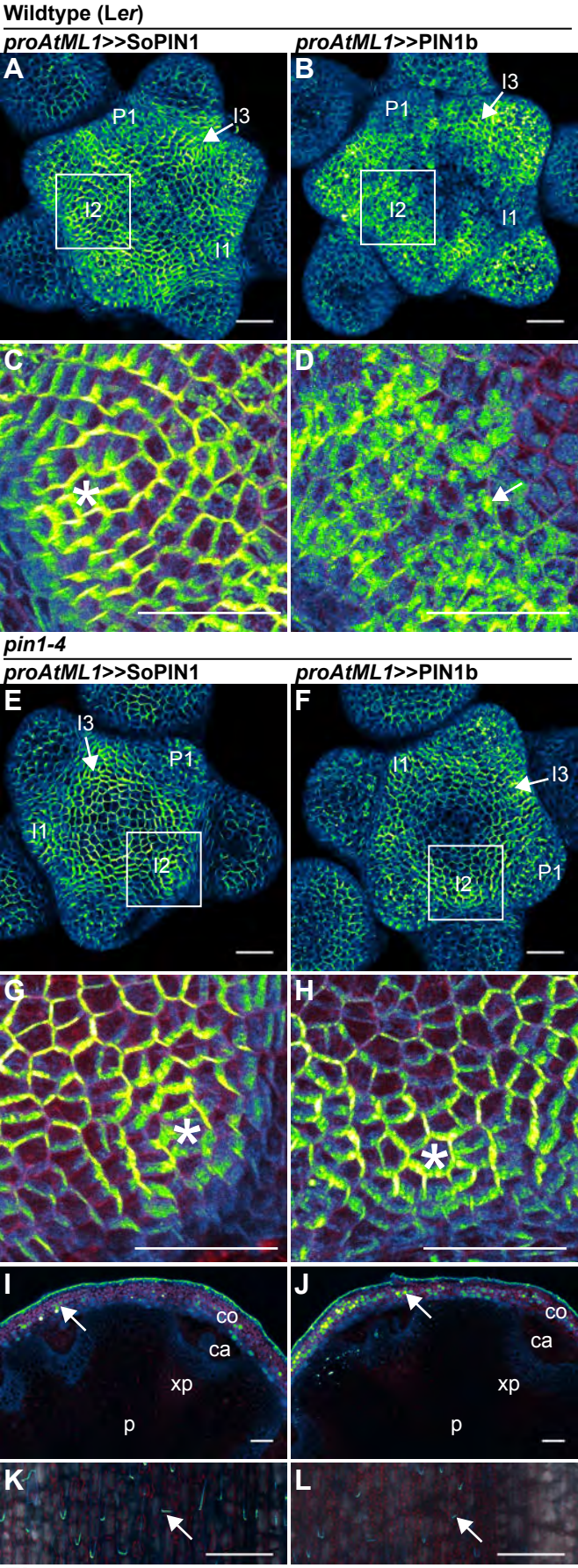
Wildtype (Ler)
proAtML1>>SoPIN1
proAtML1>>PIN1b
A
B
P1
I3
I2
I1
C
D
pin1-4
proAtML1>>SoPIN1
proAtML1>>PIN1b
E
F
G
H
I
J
co
ca
xp
p
K
L

Figure 6

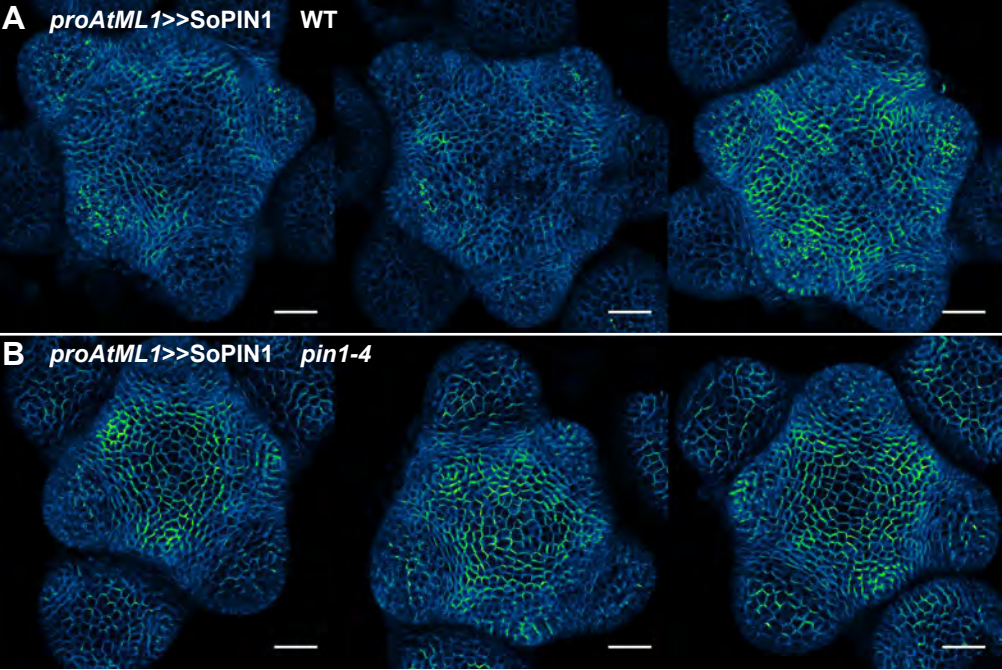

Figure 6 - supplement 1 - *proAtML1*>>SoPIN1

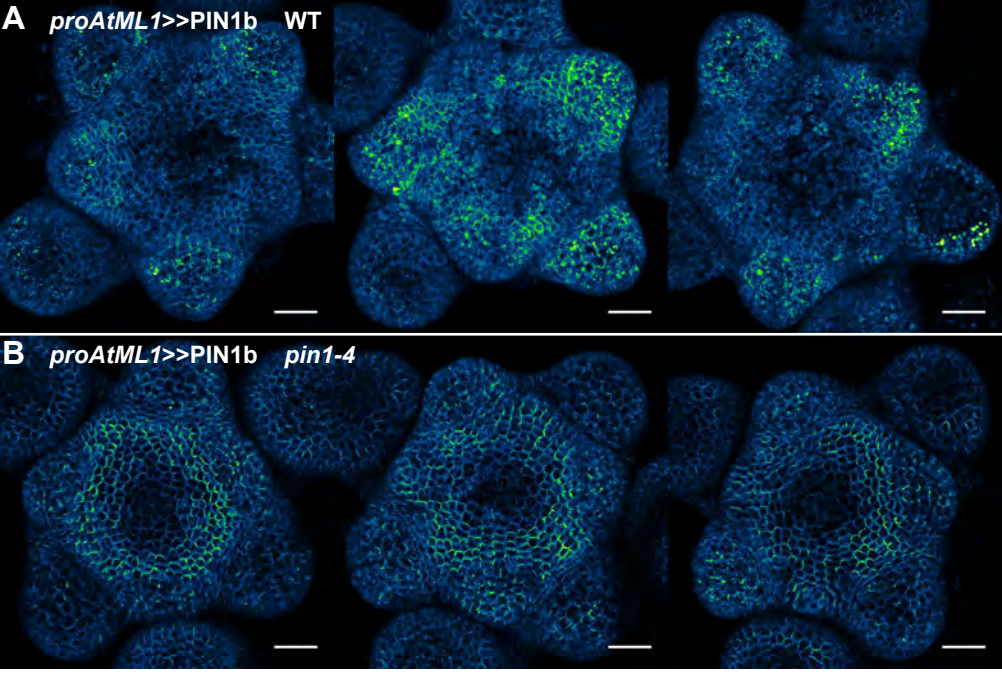

Figure 6 - supplement 2 - *proAtML1*>>PIN1b

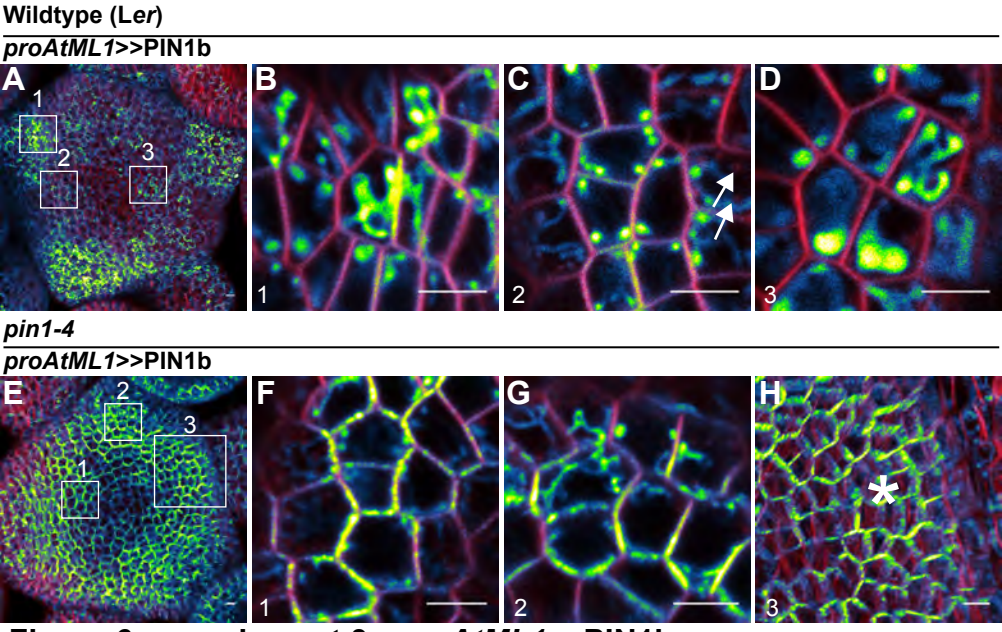

Figure 6 - supplement 3 - *proAtML1*>>PIN1b

1257 **Figure 7. AtPIN1 protein immuno-localization in wild-type, *pin1-613,* and *pin1-4***
1258 **meristems. (A)** AtPIN1 protein accumulation in wild-type L*er* inflorescence apex shows
1259 polar PIN protein at the sites of initiating organs (asterisk), and during vein patterning
1260 below the apex (arrow). **(B)** No AtPIN1 protein is detected in *pin1-613* null mutant pin-
1261 formed apexes. **(C)** Abundant AtPIN1 protein is detected in *pin1-4* pin-formed apexes,
1262 primarily in provascular tissues below the meristem apex (arrow). Box shows region of
1263 detail in **(D). (D)** Detail of boxed area shown in **(C)**. AtPIN1 protein in *pin1-4*
1264 accumulates in a perinuclear domain (arrow). All samples are 9μm longitudinal sections.
1265 Scale bars: 25μm in A-C, and 5μm in D.

1266

1267

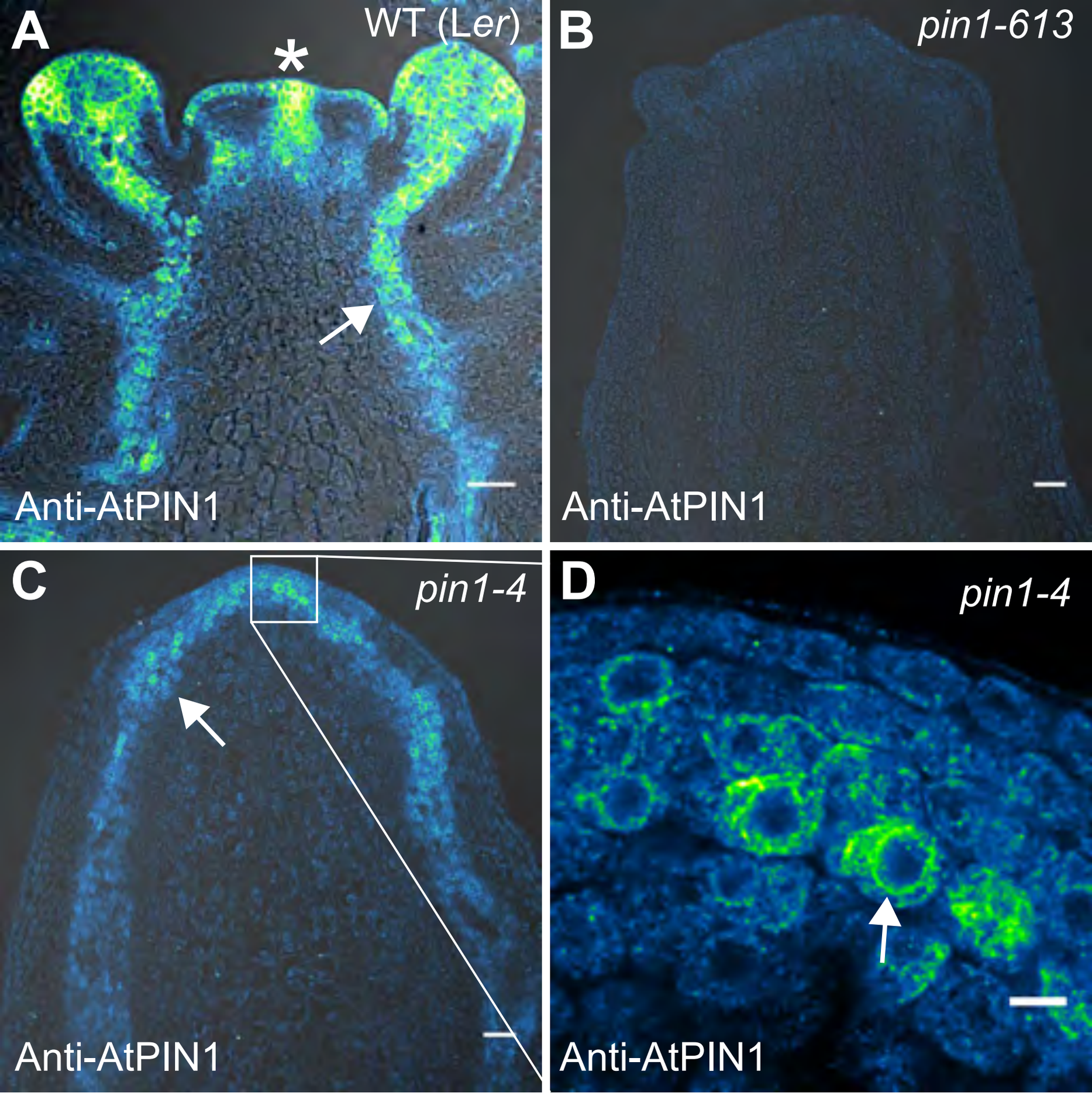
A
WT (Ler)
*
Anti-AtPIN1
B
pin1-613
Anti-AtPIN1
C
pin1-4
Anti-AtPIN1
D
pin1-4
Anti-AtPIN1

Figure 7

1268 **Figure 8. Both SoPIN1 and PIN1b can complement Arabidopsis *pin1-4* under**
1269 ***proAtML1*-driven expression. (A)** From left to right, wild-type L*er, proAtML1*>>PIN1b
1270 complemented *pin1-4, proAtML1*>>SoPIN1 complemented *pin1-4, and pin1-4 alone.*
1271 Arrow indicates barren pin inflorescence in *pin1-4*. See Figure 8 – supplement 1 for
1272 inflorescence phenotypes. **(B)** Box-plot of bulk auxin transport (counts per minute,
1273 CPM) through basal internodes 1cm above the rosette of 40-day-old Arabidopsis
1274 inflorescence stems (n=16 each genotype). Samples with different letters are
1275 significantly different from each other (ANOVA, Tukey HSD, $p < 0.05$). See Figure 8 -
1276 Source Data 1 for source data. **(C)** Box-plot of stem cross-sectional area (square mm)
1277 of the basal internode 1cm above the rosette (n=12 each genotype). Samples with
1278 different letters are significantly different from each other. (ANOVA, Tukey HSD, $p <$
1279 0.05). See Figure 8 - Source Data 2 for source data. Representative Toluidine Blue O
1280 stained hand cross-sections are shown above each box for each genotype. Scale bars:
1281 1cm in **(A)**. 500µm in **(C).**
1282
1283 **Figure 8 – supplement 1. *proAtML1*>>SoPIN1 and *proAtML1*>>PIN1b**
1284 **complemented *pin1-4* inflorescence phenotypes. (A)** Wild-type L*er*, **(B)**
1285 *proAtML1*>>SoPIN1 complemented *pin1-4,* and **(C)** *proAtML1*>>PIN1b complemented
1286 *pin1-4* inflorescence apexes. Scale bars: 1mm.
1287
1288 **Figure 8 - Source Data 1. Source data for Figure 8B auxin transport assays.**
1289

1290 **Figure 8 - Source Data 2. Source data for Figure 8C stem cross-sectional area**

1291 **measurements.**

1292

1293

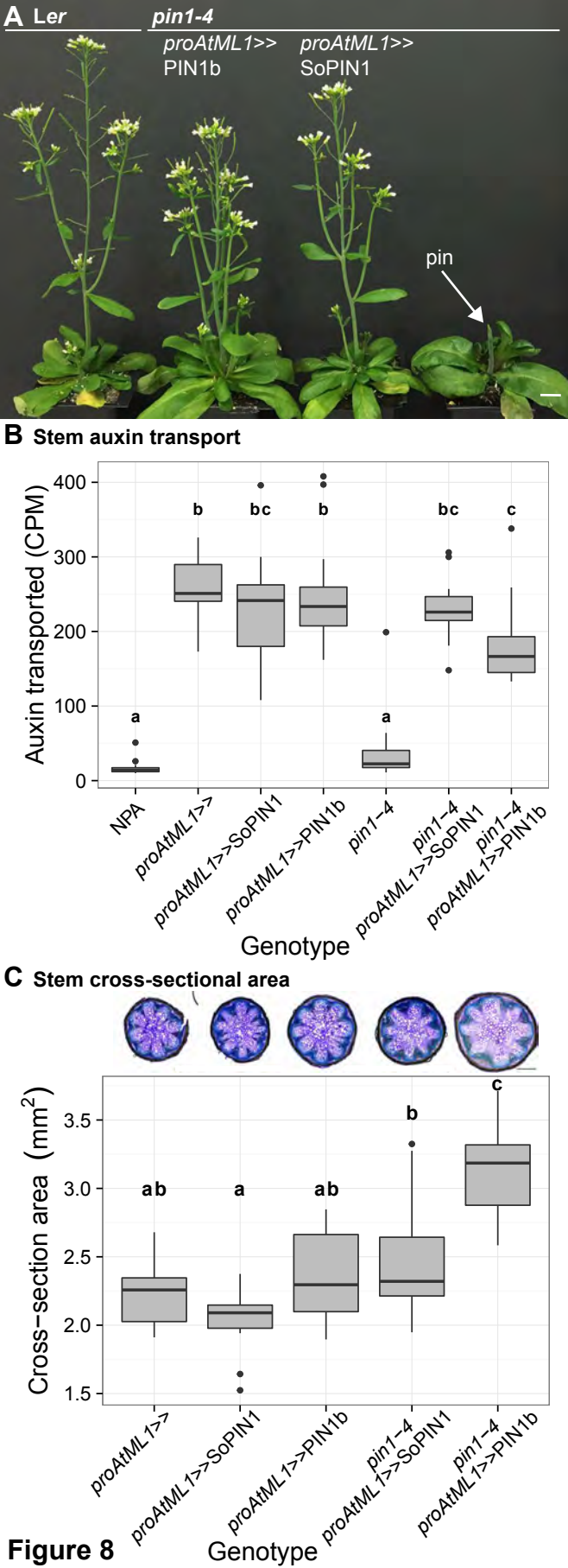
A
Ler
pin1-4
proAtML1>>
PIN1b
proAtML1>>
SoPIN1
pin
B
Stem auxin transport
Auxin transported (CPM)
400
300
200
100
0
a
b
bc
b
a
bc
c
NPA
proAtML1>>
proAtML1>>SoPIN1
proAtML1>>PIN1b
pin1−4
pin1−4
proAtML1>>SoPIN1
pin1−4
proAtML1>>PIN1b
Genotype
C
Stem cross-sectional area
Cross−section area (mm2)
3.5
3.0
2.5
2.0
1.5
ab
a
ab
b
c
proAtML1>>
proAtML1>>SoPIN1
proAtML1>>PIN1b
pin1−4
proAtML1>>SoPIN1
pin1−4
proAtML1>>PIN1b
Genotype

Figure 8

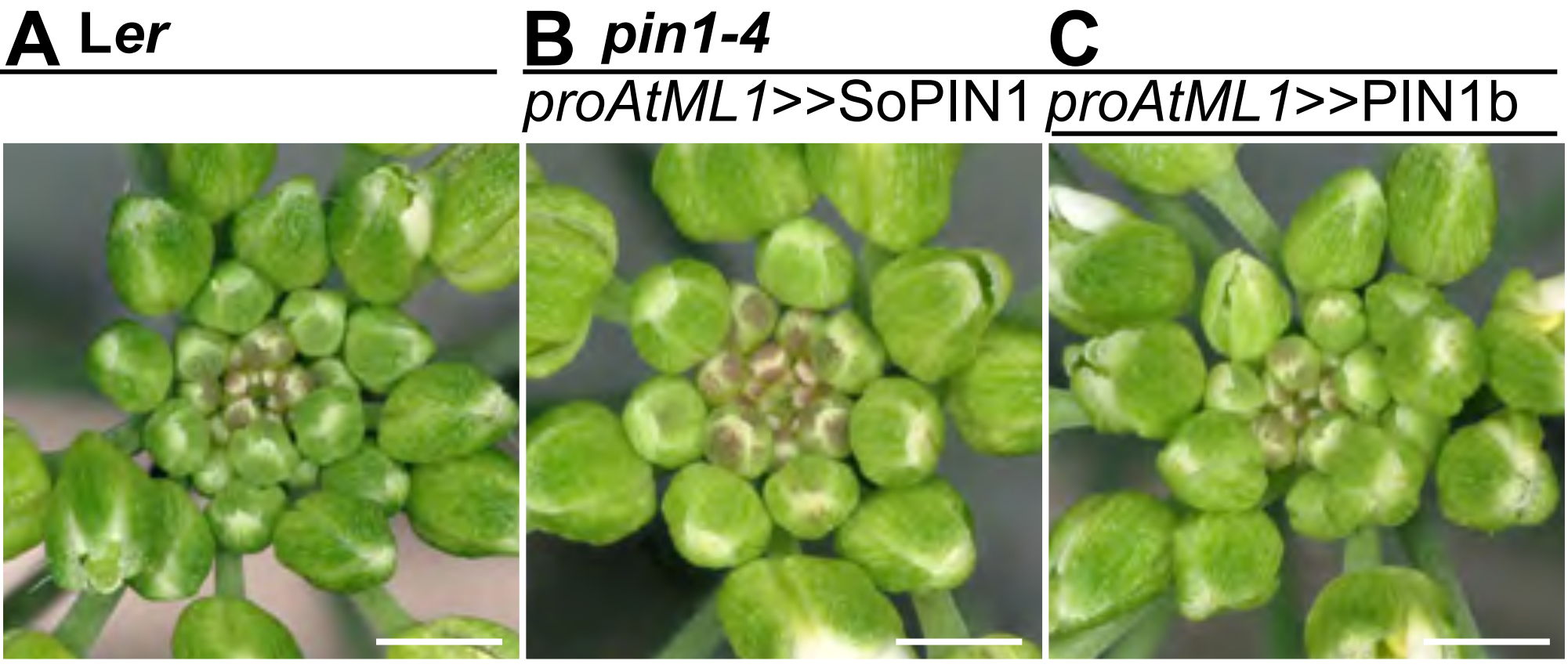

Figure 8 - supplement 1

1294 **Figure 9. Heterologous expression visual summary: Functional distinction**
1295 **between PIN auxin efflux proteins during development.** Polarized SoPIN1 is
1296 represented by green lines, polarized PIN1b by blue lines, un-polarized PIN1b by blue
1297 circles, and the putative partially functional *pin1-4* protein is indicated by magenta
1298 circles. Red arrows indicate measured auxin transport in the basal internode, while red
1299 bar-headed lines indicated reduced transport. Black arrows represent polarized PIN
1300 patterns. Convergence points are marked with asterisks. **(A)** When expressed in both
1301 the epidermis and internal tissues with *proAtPIN1* in wild-type Col-0, SoPIN1 forms
1302 convergent polarization patterns in the epidermis and is partially able to rescue the
1303 organ initiation phenotypes and bulk transport in null *pin1-613* mutants. **(B)** When
1304 SoPIN1 is expressed only in the epidermis from the *proAtML1* promoter, it forms
1305 convergence points in the wild-type background and is able to rescue more fully the
1306 organ initiation phenotypes of the *pin1-4* single amino acid change mutation in L*er.* **(C)**
1307 In contrast, when PIN1b is expressed in both the epidermis and internal tissues from the
1308 *proAtPIN1* promoter in wild-type Col-0, it accumulates mostly in the internal tissues, and
1309 is unable to complement the *pin1-613* organ initiation phenotype. It is also unable to
1310 transport auxin through stem segments, despite apparently AtPIN1-like accumulation
1311 and polarization in the stem. **(D)** When PIN1b is expressed in the epidermis from the
1312 *proAtML1* promoter it does not form convergent polarization patterns and is often un-
1313 polarized in the wild-type *Ler* background (blue ovals), but it does in the *pin1-4*
1314 background, where it is able to rescue the defective organ initiation phenotype and
1315 mediate bulk transport. See Figure 9 - supplement 1 for a protein alignment comparing
1316 AtPIN1 to other PIN1-clade protein sequences from diverse angiosperms.

1317

1318 **Figure 9 - supplement 1. Brassicaceae-specific PIN1 domains. (A)** Wrapped protein
1319 alignment showing PIN1 clade members from across the angiosperms. Grass PIN1a
1320 proteins are indicated with grey rectangle, grass PIN1b proteins are indicated with black
1321 rectangle, and Brassicaceae PIN1 proteins are indicated with red rectangle. Domains
1322 that are unique to the Brassicaceae family proteins are indicated by transparent red
1323 boxes over the alignment. **(B)** Sequenced angiosperm species and version numbers,
1324 from https://phytozome.jgi.doe.gov. Species used in the alignment in **(A)** are indicated
1325 with green circles. See Figure 9 - Source Data 1 for source data.

1326

1327 **Figure 9 - Source Data 1. FASTA alignment source data for Figure 9 - supplement**
1328 **1.**

1329

1330 **Table 1. Primers.** See methods for usage.

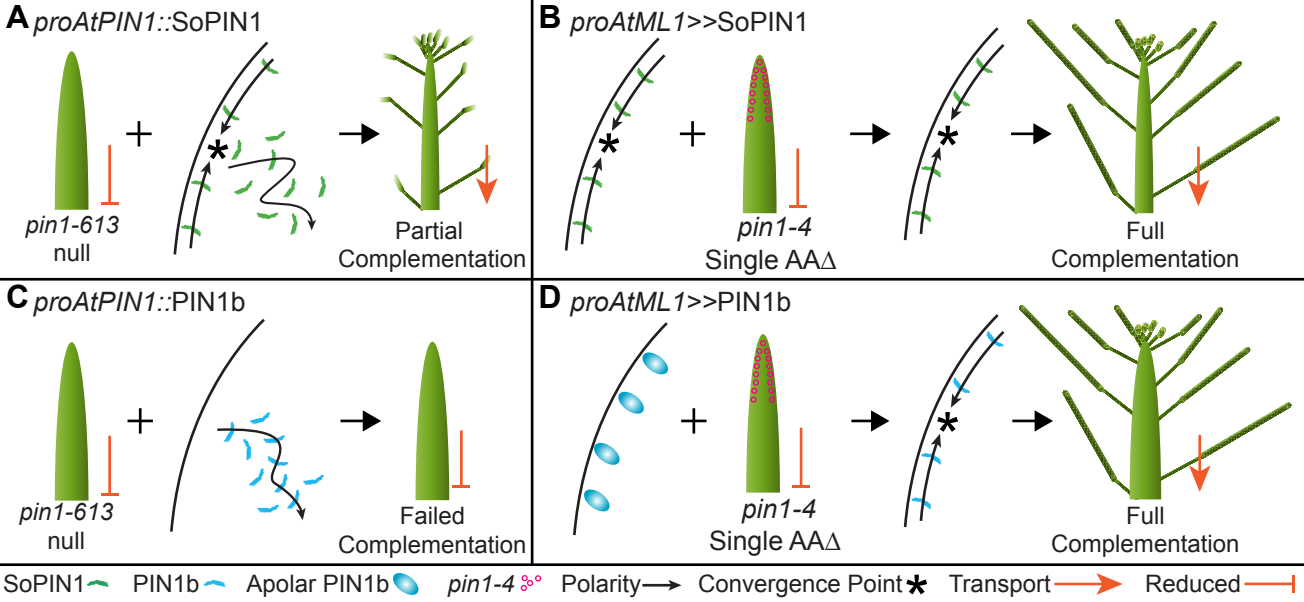
A proAtPIN1::SoPIN1
pin1-613
null
Partial
Complementation
B proAtML1>>SoPIN1
pin1-4
Single AAΔ
Full
Complementation
C proAtPIN1::PIN1b
pin1-613
null
Failed
Complementation
D proAtML1>>PIN1b
pin1-4
Single AAΔ
Full
Complementation
SoPIN1
PIN1b
Apolar PIN1b
pin1-4
Polarity
Convergence Point
Transport
Reduced

Figure 9

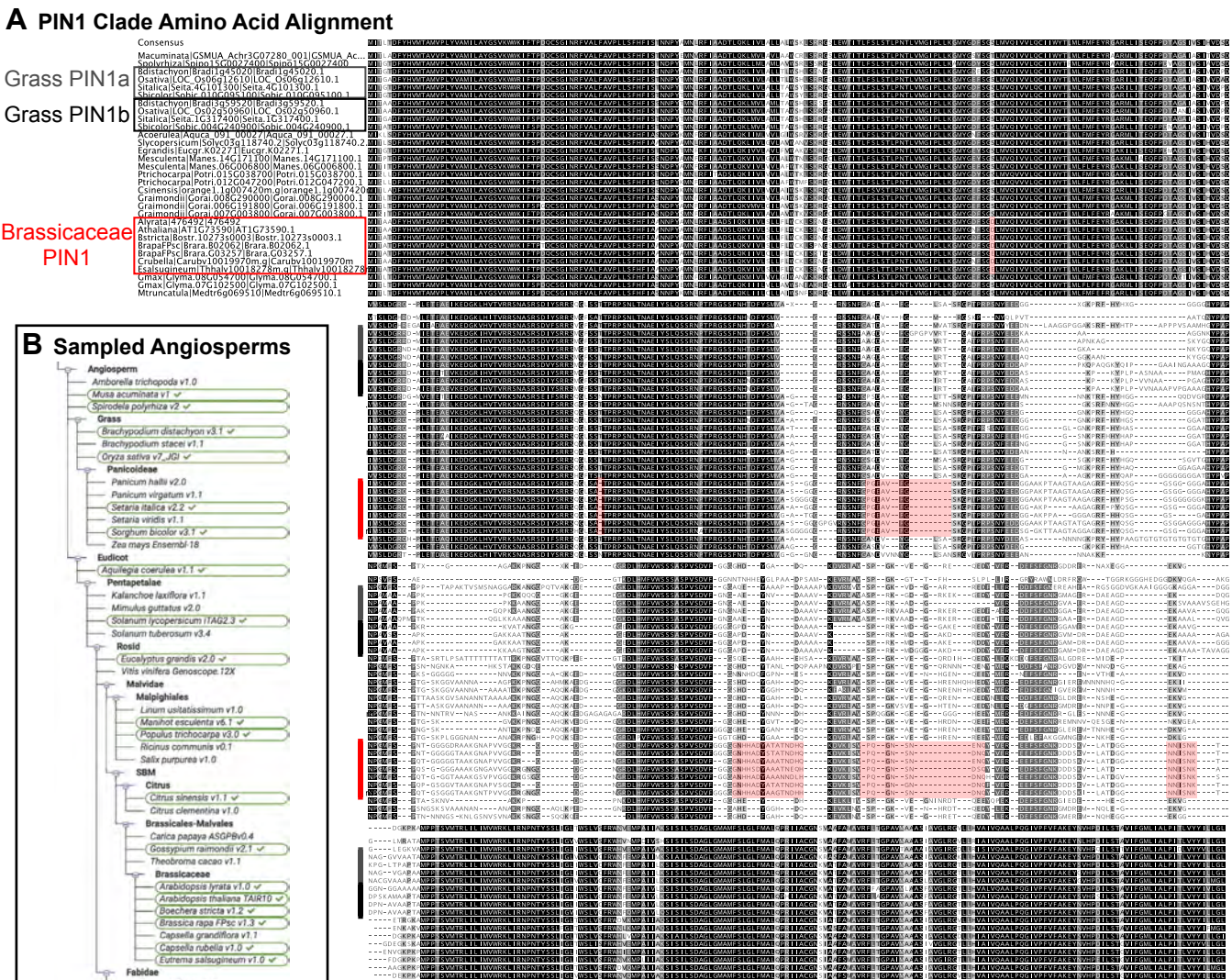

Figure 9 - supplement 1

Table 1: Primers

ID#	Name	Sequence	Purpose
1	524_Bradi4g26300_4230_F	CGTTCCGTGTTGATTCCGATG	*sopin1-1* genotyping with HgaI digestion
2	525_Bradi4g26300_4923_R	CTGGAGTAGGTGTTGGGGTTC	*sopin1-1* genotyping with HgaI digestion
3	526_Cas9_8622_F	TCCCAGAGAAGTACAAGGAGATCT	Cas9 Genotyping
4	527_Cas9_9159_R	TTGTACACGGTGAAGTACTCGTAG	Cas9 Genotyping
5	104_BdPIN_11_QPCR_F	ACAACCCTTACGCCATGAAC	*pin1a-1* genotyping with NcoI digestion
6	473_PIN1a_dom1_shortR	CACACGAACATGTGCAGGTC	*pin1a-1* genotyping with NcoI digestion
7	541_Bradi3g59520_PIN1b_5084_F	TGATGCTCTTCATGTTCGAGTACC	*pin1b-1* genotyping with mboI digestion
8	542_Bradi3g59520_PIN1b_5838_R	GGAGTAAACTACGTTGTGACAAGG	*pin1b-1* genotyping with mboI digestion
9	019 - Ubi-1 Prom attB4 F	GGGGACAACTTTGTATAGAAAAGTTGCTGCAGTGCAGCGTGACCCGG	pZmUbi amplification for cloning
10	020 - Ubi-1 Prom attB1 R	GGGGACTGCTTTTTTGTACAAACTTGCTGCAGAAGTAACACCAAACA	pZmUbi amplification for cloning
11	PIN1pro-GW-F	GGGGACAACTTTGTATAGAAAAGTTGTTACCCTCATCCATCATTAACTT	*proAtPIN1* amplification
12	PIN1pro-GW-R	GGGGACTGCTTTTTTGTACAAACTTGTCTTTTGTTCGCCGGAGAAGAGA	*proAtPIN1* amplification
13	455 BdSoPIN1 cacc mRNA	TCACATCTGCTGCCGCTGCC	SoPIN1-Citrine coding region amplification
14	302 - PIN_7 qPCR UTR R2	AATCCCAAAAGCCGACATTG	SoPIN1-Citrine coding region amplification
15	466 BdPIN1b cacc mRNA-2	CACCTGTACACACTGCGGCGCT	PIN1b-Citrine coding region amplification
16	308 - PIN_5 qPCR UTR R1	ACTCGCTAACCAACCCCTTAATT	PIN1b-Citrine coding region amplification
17	MVR087 - pin1-613 RP (SALK_047613)	AATCATCACAGCCACTGATCC	*pin1-613* genotyping
18	MVR086 - pin1-613 LP (SALK_047613)	CAAAAACACCCCCAAAATTTC	*pin1-613* genotyping
19	MVR036 - LBb1.3	ATTTTGCCGATTTCGGAAC	*pin1-613* genotyping
20	344 - Citrine Seq R	GAAGCACATCAGGCCGTAG	PIN1b-Citrine and SoPIN1-Citrine genotyping
21	524_Bradi4g26300_4230_F	CGTTCCGTGTTGATTCCGATG	SoPIN1-Citrine genotyping
22	541_Bradi3g59520_PIN1b_5084_F	TGATGCTCTTCATGTTCGAGTACC	PIN1b-Citrine genotyping
23	543_pin1-4_Aci_F	GCTTTTGCGGCGGCTATGAGATTTGT	*pin1-4* genotyping with AciI digestion
24	544_pin1-4_Aci_R	GCTTCTGATTTAATTTGTGGGTTTTCA	*pin1-4* genotyping with AciI digestion
25	076 - BASTA_F2	CTTCAGCAGGTGGGTGTAGAG	ML1::LhG4 genotyping
26	077 - BASTA_R2	GAGACAAGCACGGTCAACTTC	ML1::LhG4 genotyping